Femtosecond lasers in gas phase chemistry

R. E. Carley, E. Heesel and H. H. Fielding*

Received 25th August 2005
First published as an Advance Article on the web 29th September 2005
DOI: 10.1039/b509463a

This *critical review* is intended to provide an overview of the state-of-the-art in femtosecond laser technology and recent applications in ultrafast gas phase chemical dynamics. Although "femtochemistry" is not a new subject, there have been some tremendous advances in experimental techniques during the last few years. Time-resolved photoelectron spectroscopy and ultrafast electron diffraction have enabled us to observe molecular dynamics through a wider window. Attosecond laser sources, which have so far only been exploited in atomic physics, have the potential to probe chemical dynamics on an even faster timescale and observe the motions of electrons. Huge progress in pulse shaping and pulse characterisation methodology is paving the way for exciting new advances in the field of coherent control. (203 references.)

1. Introduction

Femtosecond lasers have had a major impact in the field of chemical dynamics. Molecules vibrate on a femtosecond timescale (1 fs = 10^{-15} s) so femtosecond light sources provide an ideal tool for observing molecular bonds being broken and made in real time. As well as providing the capability for monitoring chemical dynamics there is a current trend towards exploiting femtosecond lasers to control chemical reactions. Specifically engineered femtosecond light pulses can steer a chemical reaction towards a preferred product at the expense of unwanted side products and starting material.

Femtosecond laser experiments generally employ pump–probe techniques in which the pump laser pulse either initiates a chemical reaction or creates a non-stationary state also known as a wave packet. A probe pulse is then fired at a series of well-timed intervals after the pump pulse and is configured to generate an observable that will provide information about the evolving system. Precisely what dynamical information can be retrieved from a pump–probe scheme is highly dependent on the excitation scheme and the observation method, and so a

Department of Chemistry, University College London, 20 Gordon Street, London WC1H 0AJ, UK. E-mail: h.h.fielding@ucl.ac.uk

Robert Carley

Robert Carley was awarded a BA in Fine Art from Sheffield Hallam University and then an MSci in Chemistry from King's College London in 2000. His PhD work, conducted in the group of Professor Helen Fielding at University College London, was concerned with coherent control of atomic Rydberg electronic wave packets and vibrational wave packets in diatomic molecules, and was completed in 2005. He is currently a postdoctoral researcher in the same group working on the coherent control of organic photochemistry.

Eva Heesel

Eva Heesel obtained her first degree in Astrophysics and Physics from Queen Mary and Westfield College, University of London. She did her PhD on interaction of small molecules with short intense laser pulses under the supervision of Professor Jon Marangos at Imperial College London. After completing her PhD in 2004, she was appointed as a postdoctoral researcher in the group of Professor Helen Fielding at University College London. Her research interests include the interaction of atoms and molecules with femtosecond and attosecond laser pulses.

Helen Fielding

Helen Fielding obtained her first degree from Cambridge in 1989, and carried out her PhD with Professor Tim Softley at Cambridge and then Oxford on the spectroscopy of Rydberg atoms and small molecules in external electric fields. She did her postdoctoral research on Rydberg wave packets in external electric and magnetic fields with Professor Ben van Linden van den Heuvell at the University of Amsterdam. She moved to King's College London in 1994 and then to University College London in 2003. She received the Royal Society of Chemistry Harrison Memorial Prize in 1997 and the Marlow Medal in 2001.

great deal of effort is directed towards developing innovative detection schemes to map out as much of the dynamical pathway as possible. A very basic detection scheme is transient absorption spectroscopy, which is widely applicable in condensed phase systems. For isolated molecules in the gas phase, laser induced fluorescence and multiphoton ionisation have been popular techniques due to the ease with which they are employed. However, these methods rely on the system under investigation having the right energy level structure, and since the energy level structure usually evolves with time, this limits the observation window to a small portion of the reaction coordinate. Time-resolved photoelectron spectroscopy, however, is emerging as a powerful technique for following the dynamics of isolated molecules, ions and clusters along the entire reaction coordinate. Ionisation is a universal probe and the photoelectron spectrum is sensitive to both the electronic and nuclear configuration. What is more, using imaging techniques, it is also possible to probe the evolution of the angular distribution of the photoelectrons providing additional information about the evolution of angular momentum of the system. Another revolutionary method for following the dynamics of a reaction once it has been initiated is ultrafast X-ray or electron diffraction.

The application of femtosecond lasers to probe molecular dynamics is not a new field, it was pioneered by the groups of Gerber and Zewail more than 20 years ago, and was recognised by the award of the Chemistry Nobel Prize to Zewail in 1999.[1] There has been an explosion in activity in this field during the last decade and many important applications in diverse areas of chemistry ranging from the photochemistry of isolated organic and inorganic molecules to the dynamics of clusters, the photobiology of vision, DNA radiation damage and photosynthesis, and molecular photoelectronics. Because of this huge interest the field has been reviewed extensively elsewhere.[2,3] The purpose of this particular critical review is to provide an overview of the tools and techniques that have become available during the last few years, to review the current status of gas phase femtosecond spectroscopy and coherent control and speculate on what the future holds.

2. Femtosecond lasers

Femtosecond laser technology is a research field in itself and there are many excellent reviews, see for example.[4–7] This section is intended to provide an introduction to femtosecond lasers for the chemist. It explains the basics and the current state-of-the-art.

2.1 The basics

A laser cavity in its simplest form consists of a gain medium, and one mirror at each end of the cavity. Radiation that travels in the cavity and is reflected by the mirrors, gains energy and hence amplification on each pass through the gain medium. The principle behind this amplification process is stimulated emission of photons from an excited state, which gave rise to the word 'laser' as an acronym for 'Light Amplification by Stimulated Emission of Radiation'. The medium is 'pumped' in order to achieve a population inversion, *i.e.* an upper level is populated more than the ground state, so that stimulated emission can take place subsequently. One of the cavity mirrors has a reflectivity less than 100%, so that the radiation can leave the cavity. In order to obtain short light pulses, the radiation needs to be confined in the cavity for a number of passes before being released in a powerful pulse. Q-switching, where 'Q' refers to the quality or loss factor of the laser resonator typically generates pulses of 10–100 ns. To obtain shorter pulses, the different frequencies, or oscillation modes, that propagate in the laser cavity must be mode-locked, *i.e.* oscillate in phase with one another. Mode-locked lasers have produced pulses shorter than 5 fs.[8,9] The shortest pulse that can be obtained in principle corresponds to a single oscillation of the electric field under the pulse envelope, *i.e.* if the laser has a central wavelength of 780 nm, one oscillation corresponds to 2.6 fs. In order to generate sub-femtosecond pulses, the wavelength of the light has to be shorter; this has been demonstrated by Paul and co-workers[10] who achieved pulses as short as 250 *as* (1 *as* or attosecond = 10^{-18} s) at wavelengths shorter than 100 nm.

For linearly polarised light, the electric field can be described by $E(z,t) = \hat{\mathbf{e}}E_0 \cos(\omega t - kz)$, where $\hat{\mathbf{e}}$ specifies the polarisation (*i.e.* electric field oscillation) direction, E_0 is the amplitude, ω is the angular frequency of the radiation, $k = 2\pi/\lambda$ is the wave number (*i.e.* the number of waves per unit length), λ is the wavelength, and z is the propagation direction. The argument $(\omega t - kz)$ is also called the phase.

2.2 Pulse duration and bandwidth

The minimum pulse duration of a laser is determined by the bandwidth of the gain medium, which is commonly defined as the difference between the lowest and highest frequencies at the full width at half maximum (FWHM) signal level of the laser pulse. The product of pulse duration and laser bandwidth, called the time-bandwidth product, is given by $\Delta v \Delta\tau \geqslant K$, where Δv is the FWHM frequency bandwidth, $\Delta\tau$ is the FWHM pulse duration, and K is a constant that depends on the pulse shape ($K = 0.441$ for a Gaussian pulse and $K = 0.315$ for a sech^2 pulse). For a transform-limited pulse, *i.e.* a pulse that has the minimum possible duration for a given bandwidth, the temporal pulse profile $\Delta\tau$ is the Fourier transform of the spectral bandwidth Δv, and $\Delta v \Delta\tau = K$.

Historically, short pulses have been produced by dye lasers; these gain media typically have bandwidths of the order of 20–30 nm and support $\sim$30 fs pulses, although in specific circumstances, organic dyes have produced pulses as short as 6 fs.[11] Dye lasers have disadvantages such as instability due to photochemical degradation, thermal effects and jet flow problems. Nowadays solid state lasers are the most common laboratory femtosecond light sources. The gain medium is usually composed of transition metal ions (such as Ti^{3+}, Cr^{3+}, and Cr^{4+}) that are doped into suitable host crystals. Titanium-doped sapphire (Ti^{3+}:Al_2O_3), or Ti:Sapphire, has the largest tunability of any solid-state laser, with about 450 nm centred around 780 nm. The large gain bandwidth supports pulse durations less than 5 fs as was first demonstrated by Sutter *et al.*[8] and Morgner *et al.*[9] Strong absorption in the 532 nm wavelength range allows Ti:Sapphire to be pumped by the output of a frequency-doubled Nd:YAG laser. Additional

desirable properties of Ti:Sapphire are a high saturation fluence of about 1 J cm^{-2}, that ensures efficient extraction of energy from the gain medium, and a high thermal conductivity that permits the gain medium to be pumped at a high repetition rate, which is especially important for the amplification of the laser pulses. It should be noted that the large saturation fluence can cause Q-switching instabilities; moreover the operating efficiency is low, and the emission wavelength is not well matched to telecommunication applications. In practice, Ti:Sapphire lasers are often used in research laboratories, while other short pulse laser types are used for commercial, medical and telecommunication applications. These other laser types include diode (or semiconductor) lasers, such as current-modulated vertical cavity surface emitting lasers (VCSELs) and optically pumped vertical external cavity surface emitting lasers (VECSELs), and fibre lasers (which can produce sub-picosecond pulses (where 1 picosecond is 10^{-12} seconds) using a semiconductor saturable absorber mirror (SESAM), see[12,13] and references therein.

The recent development of free-electron lasers (FELs) has opened the possibility of producing sub-picosecond pulses at wavelengths that can potentially be shorter than 1 nm; a recent review was written by Feldhaus *et al.*[14] However, the operating principle of these lasers implies very large and expensive systems and hence limits them to be housed in large national research laboratories. For the rest of section 2 all the techniques refer to the Ti:Sapphire femtosecond laser system, which is the only laser system to date to produce 5 fs pulses.

2.3 Mode-locking

In a laser cavity, the emitted radiation is limited to the resonant frequencies defined by the cavity length. These frequencies or modes are separated by $\delta\nu = c/2L$, where c is the speed of light and L the optical cavity length. The mode spacing is the reciprocal of the cavity round-trip time. The spectral bandwidth of the laser transition over which optical gain is provided limits the number of longitudinal modes that can oscillate in the laser cavity. For short pulse generation, these modes must be locked in phase, which is referred to as mode-locking.

There are different mode-locking techniques, which can be classified as active or passive. In active mode-locking the radiation in the cavity is modulated at a rate which is matched to the cavity round-trip time. In passive (or self) mode-locking the laser radiation itself generates a modulation by a nonlinear process. Examples are interaction with a saturable absorber or with an optical Kerr medium. In a fast saturable absorber, the absorber recovery time is shorter than the laser pulse duration, which leads to pulse compression down to the absorber recovery time of typically a few picoseconds. A combination of a slow absorber (whose absorber recovery time is longer than the laser pulse duration) and a saturable amplifier can generate pulses that are shorter than the absorber recovery time. Very short pulse durations of a few femtoseconds can be obtained by using a saturable absorber medium that exhibits the optical Kerr effect. The optical Kerr effect, which has a very fast response of about 1 fs, is the change in the refractive index of a medium induced by an incident electric field, $n = n_0 + n_2 I$, where n_0 is the linear refractive index, n_2 is the nonlinear refractive index, and I is the laser intensity. The nonlinear refractive index is typically small ($n_2 = 4.7 \times 10^{-19}$ cm^2 W^{-1} in air, and $n_2 = 3.1 \times 10^{-16}$ cm^2 W^{-1} in Ti:Sapphire), so that a high electric field is required.

For a pulse with intensity variations across the temporal and spatial profile, different parts of the pulse experience a different response of the optical Kerr medium. In the spatial domain, a Gaussian shaped pulse (which has the highest intensity at its centre) will experience a positive lens, leading to self-focusing. In a laser cavity this can lead to passive mode-locking, and this technique is known as Kerr-lens mode-locking (KLM). KLM is not self-starting, as the initial intensity fluctuations in a laser cavity are usually not sufficiently strong to experience self-focusing. An additional noise spike that initiates mode-locking can be introduced in a number of ways, as described by French[5] and references therein; one common method is to tap one of the mirrors or prisms in the cavity. Self-focusing can become a problem, as the increase in pulse intensity induces a stronger positive lens, which in turn leads to more focusing. The corresponding power density can cause material damage or formation of beam filaments if the intensity profile has spikes. This has major implications for pulse amplification which are discussed further in section 2.5.

2.4 Propagation

As explained in section 2.2, short laser pulses have a broad bandwidth, which needs to be maintained during the pulse propagation and amplification that is necessary for most applications. The first hurdle to the preservation of the bandwidth and hence pulse duration is dispersion, which causes a temporal separation of the light wave into its different frequencies, as each frequency propagates at a different speed. The average (or carrier) frequency of the pulse propagates at the so-called phase velocity, while the modulating pulse envelope moves at the group velocity. The dispersion relation for waves is $k = n(\omega)\omega/c$, where $k = 2\pi/\lambda$ is the wave number (*i.e.* the number of waves per unit length), λ is the wavelength, ω is the angular frequency of the radiation, n is the refractive index, and c the speed of light in free space. The refractive index is the ratio of speed of light in free space to that in a medium, *i.e.* $n = c/v_{medium}$. In vacuum, the phase velocity $v_p = \omega/k$ and the group velocity $v_g = d\omega/dk$ are constant and equal to c. In optical media, n is a function of ω, so v_p and v_g are both functions of ω and different from each other. In this case, dispersion occurs, which leads to a temporal spread of the component frequencies. The rate of change of group velocity with wavelength λ is given by $dv_g/d\lambda = (\omega^2 v_g^2/2\pi c) d^2k/d\omega^2$, where $d^2k/d\omega^2$ is the group velocity dispersion (GVD), which is given by $d^2k/d\omega^2 = (\lambda_0^3/2\pi c) d^2n/d\lambda^2$, where λ_0 is the central wavelength.

A short pulse has a large bandwidth, so the temporal stretch will be high. For example, a 30 fs $sech^2$ transform-limited pulse will be stretched to 56 fs when passing though 1 cm of BK 7 optical glass. The change of frequency with time is called 'chirp', if the frequency increases with time it is called a

positive chirp and if it decreases with time it is called a negative chirp. Most materials that are used in a laser system exhibit 'normal' dispersion, *i.e.* a positive GVD, which gives rise to a positive chirp.

For the generation of sub-100 fs pulses, it is particularly important to control the GVD inherent in the oscillator cavity. In a linear system, the phase added by an optical material is given by $\phi(\omega) = -n(\omega)\omega_0 L/c$, where ω_0 is the centre angular frequency and L is the length of the material. The phase can be expanded as a Taylor expansion about the central laser frequency $\phi(\omega) = \phi(\omega_0) + \phi'\delta\omega + \frac{1}{2}\phi''\delta\omega^2 + \ldots$, where $\delta\omega = (\omega - \omega_0)$. The first term, $\phi(\omega_0)$, is the static accumulated phase, the second term is the linear phase or total group delay, the third term is the quadratic phase or linear chirp, and the fourth term is the third order phase or second order chirp. ϕ'' is also called the group delay dispersion (GDD), and is related to the GVD by $\phi'' = -Ld^2k/d\omega^2$. The higher order terms in the Taylor expansion become increasingly important with decreasing pulse duration and increasing bandwidth. The linear chirp caused by the material GVD can be compensated for by elements that provide adjustable (negative) GVD, as described below. The higher order chirps are very difficult to compensate for. The development of chirped dielectric mirrors whose multilayer structure results in a wavelength-dependent penetration depth of incident radiation has been successful in the dispersion control of ultrashort pulses.[15,16] Treacy[17] showed that negative GVD can be provided by angular dispersion using a pair of diffraction gratings, while Fork[18] demonstrated the same principle using pairs of prisms. In general, prisms provide a small net GVD and small losses, while diffraction gratings can introduce a much higher GVD but suffer from large losses. The prism arrangement is often used inside the laser oscillator, and gratings are employed in the stretcher and compressor of a chirped pulse amplifier (CPA) laser system, as described below.

Self-phase modulation (SPM) is the temporal analogue to self-focusing. The intensity distribution $I(t)$ of the laser pulses is a function of time and induces a time-dependent refractive index, $n(t) = n_0 + n_2 I(t)$, that produces a time-dependent phase change $\Delta\phi(t) = n_2\omega_0 I(t)Lt/c$. For a pulse propagating in an optical medium of length L, the accumulated phase results in an instantaneous frequency shift $\Delta\omega(t) = -n_2(\omega_0 L/c)dI(t)/dt$. This frequency shift gives rise to new frequency components which broadens the pulse spectrum. For a laser pulse with a Gaussian temporal profile, the chirp associated with $\Delta\omega(t)$ will be approximately linear in the central part of the pulse and nonlinear in the wings. Temporal phase variations in a laser pulse can be amplified by SPM and lead to a break-up of the beam. This effect is similar to that in the spatial domain, where the spatial intensity variations are amplified in self-focusing.

The large bandwidth of an ultrashort pulse must be maintained during propagation and amplification processes in order to preserve the pulse duration. This requires the optical components to have flat wavelength dependence across the laser bandwidth. In an ultrashort pulse laser system, the gain materials in the amplifier and oscillator are usually the same. For Ti:Sapphire, the gain profile is approximately Gaussian and centred around 780 nm. If the centre of the gain spectral profile does not coincide with the centre of the seed spectral profile, then the amplified spectrum will be shifted towards the centre of the gain spectrum; this is known as gain shifting. A description of gain narrowing and gain shifting together with experimental results is given by Le Blanc *et al.*[19]

2.5 Amplification

The output from a KLM laser oscillator is typically a train of femtosecond pulses at a repetition rate of about 100 MHz and pulse energy of a few nJ. For many applications, the pulse energy needs to be higher. Direct amplification of femtosecond laser pulses to high intensities leads to nonlinear pulse degradation and material damage, due to self-phase modulation and self-focusing. In order to avoid these effects, high-energy beams must have either a large area and/or long pulse duration prior to amplification. The costs (and space requirements) of large optics limits the use of large beams and restricts them to national facilities (*e.g.* the Rutherford Appleton Laboratory in the United Kingdom and the Lawrence Livermore National Laboratory in the United States). The chirped pulse amplification (CPA) technique, developed by Strickland and Mourou in 1985,[20] stretches the pulse temporally prior to amplification. A temporal stretch is achieved by propagating the femtosecond pulses through a dispersive delay line, resulting in chirped pulses. If the dispersive delay line consists of a diffraction grating pair, the incoming pulses will be spectrally dispersed, and the frequency components have different path lengths. The large bandwidth of femtosecond pulses enables temporal stretching by a large factor (typically 10^4–10^5). These chirped pulses can be amplified and then subsequently recompressed using another pair of diffraction gratings as a dispersive delay line that compensates the initial chirp by providing chirp of the opposite sign. The first diffraction grating compressor was designed by Treacy in 1968.[21]

The stretcher in a CPA system requires a system that adds chirp of opposite sign to that in the compressor. Martinez[22,23] designed such a system, based on two antiparallel diffraction gratings, with a unit magnification telescope between the gratings. The unit magnification telescope produces an effective negative separation between the gratings, such that the dispersion has equal magnitude to that in a grating compressor, but with different sign. Therefore the resulting chirp will be positive. The telescope can consist of two lenses or two mirrors. The latter arrangement is preferred in ultrashort pulsed systems, as it avoids material dispersion and chromatic aberration.

The gain medium in an amplifier is commonly also a Ti:Sapphire crystal that is pumped by, for example, a Nd:YAG laser at a repetition rate from 10 Hz up to tens of kHz. The resulting amplified pulse typically has an energy varying from a few μJ (for a very high repetition rate) to tens of mJ (for a low repetition rate), corresponding to peak intensities in the TW (1 TW = 10^{12} W) range. Fig. 1 shows a schematic of a CPA laser system. The manipulation and characterisation of the laser pulses is described in the following sections.

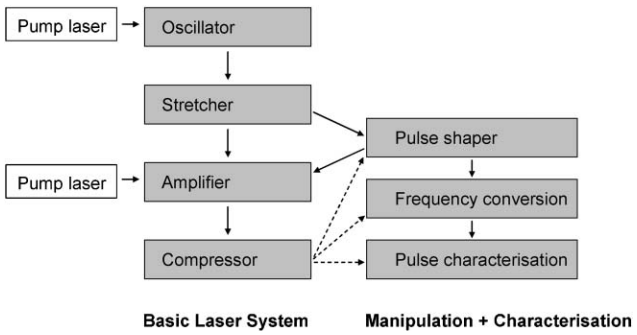

Fig. 1 Schematic of a typical amplified femtosecond laser system. Solid arrows: beam paths. Dashed arrows: optional beam paths after compressor for the manipulation and characterisation of pulses.

2.6 Few-cycle pulses

The few-cycle regime is interesting, as there are only a few oscillations of the electric field under the pulse envelope. A recent paper by Drescher and Krausz[24] provides an excellent review of the rapidly developing field of attosecond physics that exploits few-cycle pulses. Few-cycle pulses with μJ pulse energies can be obtained by focusing the laser pulse into a hollow fibre filled with a noble gas. The resulting self-phase-modulation broadens the spectrum and the resulting pulses can be compressed by chirped dielectric mirrors.[25]

The carrier-envelope offset (CEO), which is the difference between the phase of the carrier wave and the envelope position, plays a crucial role in few-cycle pulses, as it affects the number and amplitude of oscillations of the electric field under the envelope. Fig. 2a shows an example of a pulse whose peak electric field amplitude coincides with the peak of the envelope, which is called a cosine waveform and has phase $\phi = 0$. In Fig. 2b, the peak of the amplitude is shifted by $\phi = \pi/2$, resulting in a sine waveform. It should be noted that the cosine waveform has a single most intense peak, whereas the sine waveform has two equally intense peaks. The realisation of CEO control[26] has been a key achievement for the investigation of nonlinear processes, such as high-order harmonic generation (HHG) which in turn enables the production of single attosecond pulses.

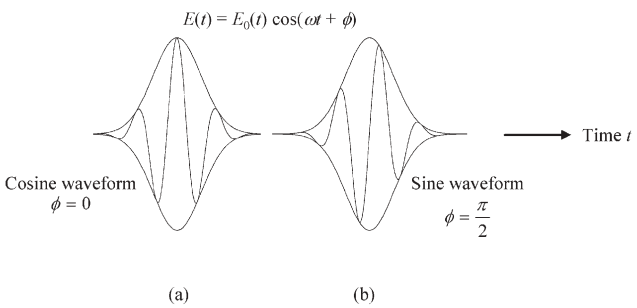

Fig. 2 Few cycle pulses with different carrier envelope phase ϕ. (a) If $\phi = 0$, the peak of the electric field $E_0(t)$ coincides with the peak of the envelope (cosine waveform). (b) If $\phi = \pi/2$, the peak of the electric field $E_0(t)$ is shifted by $\pi/2$ relative to the peak of the envelope (sine waveform).

2.7 Nonlinear optics

Common techniques for extending the wavelength coverage of high powered lasers exploit the nonlinear polarisation induced in a transparent medium at high optical electric field intensities. The polarisation is given by $\mathbf{P} = \varepsilon_0[\chi^{(1)}\mathbf{E} + \chi^{(2)}\mathbf{E}^2 + \chi^{(3)}\mathbf{E}^3 + \ldots]$, where ε_0 is the permittivity of free space, and $\chi^{(i)}$ with $i = 1,2,3\ldots$ are the electric susceptibilities. For low light intensities, $\mathbf{P}$ is linear in the electric field $\mathbf{E}$, whereas the higher order, nonlinear contributions become important with increasing intensity.

The second (lowest) order nonlinearity of non-centrosymmetric crystal materials is exploited in optical parametric amplifiers (OPAs) which are routinely employed to extend the tunability of femtosecond Ti:Sapphire lasers to the far infrared region of the spectrum. Pump beam photons, ω_p, are converted into an equal number of lower frequency signal and idler photons, $\omega_p = \omega_s + \omega_i$. The signal and idler frequencies are determined by phase matching constraints, $k_p = k_s + k_i$, which can be frequency-tuned by rotating the optical axis of the crystal. Most crystal materials are transparent over a range of more than 1000 nm; for example lithium triborate, LiB_3O_5, (commonly abbreviated as LBO) is transparent from 0.16–2.6 μm.

A special example of nonlinear optical frequency conversion is the production of harmonic frequencies at multiples of the fundamental wavelength, such as second-harmonic generation (SHG), third-harmonic generation (THG) and fourth-harmonic generation (FHG). For a fundamental wavelength of around 800 nm, the fourth harmonic order is around 200 nm, *i.e.* in the ultra-violet regime, where many materials start to absorb light. If even shorter wavelengths are to be produced, the opacity of glasses to wavelengths below ~200 nm makes it necessary to use a gas instead. By focusing the laser into a gas target, much higher odd orders can be generated; this is referred to as high-order harmonic generation (HHG). Harmonic photons with energy of more than 1000 eV, *i.e.* at a wavelength of about 1 nm, have been reported recently by Seres and co-workers.[27] This makes high-order harmonic generation attractive for applications such as X-ray imaging in the water window wavelength range of 2.4–4.4 nm; however, it should be noted that the conversion efficiency to date is only around 10^{-6}. A useful property of the high harmonic orders is their short duration that can be less than a femtosecond, which makes them suitable for initiating and controlling the motion of electrons in atoms and molecules.

Another technique involves stimulated Raman scattering of two photons in a gas target to generate new wavelengths, or "sidebands", spaced by the difference in frequencies of the incoming beams. Raman scattering has conversion efficiency close to unity and also has the potential to generate sub-femtosecond pulses.[28–30] Currently, Raman generation produces trains of pulses, whereas high-order harmonic generation can produce single pulses and therefore may be preferable for applications involving triggering or probing chemical reactions.

2.8 Pulse shaping

Recent advances in technology enable the frequency, polarisation and temporal profile of femtosecond light pulses to be

shaped arbitrarily. The field of pulse shaping is vast and has been covered in a number of excellent reviews.[31,32] Goswami[33] provides a review of pulse shaping techniques applied to coherent control. Here, we present an overview of common pulse shaping techniques.

In principle, pulse shaping is achieved by sending the input pulse through a linear, time-invariant filter whose response modulates the pulse, resulting in a shaped output field. The response of the filter has to be sufficiently fast to modulate the input pulse. For femtosecond pulses, there are no electronic devices with such capabilities, so instead the filtering is performed in the frequency domain. The frequencies of the incoming pulse may be spatially dispersed and then addressed individually by a spatial-light modulator (SLM). A basic pulse shaper consists of a pair of diffraction gratings and lenses that are arranged in a ''zero-dispersion'' 4*f* configuration, where *f* is the focal length of the lenses, as shown in Fig. 3. The first grating disperses the frequency components of the incoming light pulse which are then focused at the back focal (Fourier) plane of the first lens. The modulator is placed in the Fourier plane where it can address the different frequency components. The second lens recollimates the individual frequency components, and the grating recombines them into a single beam which constitutes the output pulse. For pulses shorter than 50 fs where dispersion becomes very important the lenses are commonly replaced by cylindrical mirrors.

Early SLMs were fixed masks, which can be machined very accurately using microlithography, but have the disadvantage of the need for a new mask every time the pulse shape has to be changed. The field has been revolutionised by the development of programmable masks such as liquid crystal arrays. These masks can be operated in an open-loop configuration, in which the mask is programmed to generate a specific pulse profile, or a closed-loop configuration in which the result of the operation of the pulse on an experiment is compared with the objective of the experiment and used as feedback to determine the optimum pulse profile.

There are three classes of programmable masks or spatial light modulators that are commercially available: liquid crystals (LC), acousto-optical modulators (AOM), and deformable mirrors. Liquid crystal modulators have been used

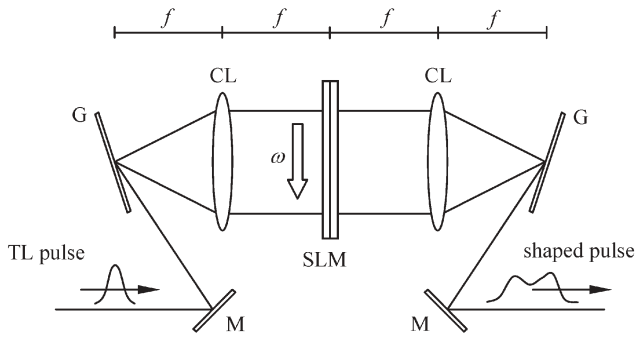

Fig. 3 Schematic of a zero-dispersion pulse shaper in a 4*f* configuration. TL: transform-limited; M: mirror; G: grating; CL: cylindrical lens with focal length *f*; SLM: spatial light modulator. The angular frequency ω changes across the SLM, enabling the addressing of individual frequency components, which results in a shaped output pulse.

for both phase-only[34,35] or phase-and-amplitude pulse shaping.[36,37] The liquid crystals are nematic, *i.e.* they consist of elongated molecules that are aligned parallel to each other. If an electric field is applied, the molecules rotate, resulting in a change of the refractive index. A liquid crystal modulator has an array of crystals sandwiched between two glass layers coated with a conducting film, such that each of the crystals acts as a pixel that can have an individual voltage applied to it. Commercially available liquid crystal SLMs currently have either 128 or 640 pixels[38] with around 100 μm centre-to-centre pixel spacing and 2–3 μm gaps between adjacent pixels. The gaps lead to pixelation, *i.e.* to a limit in resolution, as the output waveform has steps rather than being smooth. Increasing the focal spot size improves this situation, though it also decreases the spectral resolution. The pixelation problem was addressed by Dorrer *et al.*[39] who used an optically addressed liquid crystal SLM, which is also known as liquid crystal light valve. The light valve consists of continuous twisted nematic crystal layers and a photoconductive layer embedded in transparent electrodes. When the valve is illuminated with light, the voltage across the electrodes will change, such that the molecules in the liquid crystal rotate. The light valve has a limited spatial frequency response, which might make it more useful for small phase corrections rather than for large ones. Recently, a programmable phase modulator with 1024 × 768 pixels was developed by Hamamatsu that combines the advantage of an optically addressed phase modulator, that eliminates pixelation and diffraction structure, with an electrically addressed phase modulator that can be conveniently controlled by a computer.[202] Liquid crystals are efficient SLMs in the near-infrared (NIR) (*e.g.* the 800 nm fundamental of the Ti:Sapphire laser) but they are not suitable for the ultraviolet because absorption sets in below about 450 nm. Recently, Brixner and Gerber[40] demonstrated that the light polarisation, *i.e.* the oscillation direction of the electric laser field, can also be 'shaped' to have different linear and elliptical orientations with varying degrees of ellipticity within a single laser pulse.

The development of acousto-optic modulators was pioneered by Warren and co-workers,[41–44] in which the SLM consists of a crystal, usually TeO_2 for visible and InP for infrared wavelengths. The crystal is driven by a radio-frequency (rf) voltage signal, which is converted into a travelling acoustic wave by a piezoelectric transducer. The acoustic wave creates a refractive index grating that diffracts the dispersed frequency components of the laser pulse. The recent introduction of the acousto-optical programmable dispersive filter (AOPDF)[45,46] maximises the interaction length between the acoustic and optical waves by a collinear geometry. The AOPDF provides for large dispersion compensation of femtosecond laser pulses and does not need to be placed in the focal plane of the pulse shaper, which enables a more compact design. The disadvantage of AOPDFs is that the shaping of shorter wavelength pulses requires higher acoustic frequencies for which absorption is increased. However, Kaplan and co-workers[47,48] have demonstrated the possibility of extending the wavelength range down to 500 nm. Recently, Roth *et al.*[49] demonstrated acousto-optical pulse shaping of both spectral amplitude and phase for UV pulses by

using a fused silica AOM. The centre wavelength was 400 nm, but the transmission limit of fused silica could in principle, allow shaping of wavelengths down to 180 nm. A point to note is that AOM-based pulse shapers have a low overall efficiency (due to low diffraction efficiency) of about 10–15%, while liquid crystal SLMs can have an efficiency of 70% or more.

If a movable or deformable mirror is placed in the Fourier plane of the 4*f* configuration introduced, then the resulting 2*f* configuration (which will be double-passed, therefore resulting in a 4*f* geometry) can be used for phase-only pulse shaping. The deformation of the mirror is commonly achieved by applying a voltage to a number of actuators at the back of the mirror. An early approach used a mirror membrane supported over actuator elements, with a maximum displacement of 4 μm due to the electrostatic effect,[50] while Chériaux *et al.* used a micromachined deformable mirror (MMDM) that was deflected with electrostrictive actuators with a precision of 40 nm.[51] A similar approach by Radzewicz and co-workers[52] used a piezo-actuated deformable reflector (PADRE) for pulse shaping. Hacker and co-workers[53] used an array of micro mirrors, based on a micro electro mechanical system (MEMS), as a phase-modulating SLM at 400 nm. In principle, the device could be used for one- and two-dimensional phase modulation of femtosecond pulses from 200–900 nm. Femtosecond pulse shaping has also been demonstrated with a bimorph piezo-ceramic mirror.[54] Bimorph mirrors have been used in adaptive optics, which corrects for distortions of light in media (*e.g.* the effects of the Earth's atmosphere on starlight or the aberrations of the human eye), and can be fabricated at a lower cost and with much simpler processes compared to membrane mirrors. Another scheme, demonstrated by Vdovin and Loktev,[55] used the thermal expansion of resistors, though thermal fluctuations cannot be corrected; hence this scheme might be only useful for slow-changing large-scale aberrations of wavefronts.

There are a variety of other pulse shaping methods, which have been described very well in the literature.[32,33] In the context of this review, we briefly mention a technique that uses molecules as pulse shapers.[56] The idea is based on the time-dependent phase modulation induced by a molecular wave packet that can be used to manipulate the phase of ultrashort laser pulses, as well as increase their bandwidth. An attractive feature of this method is that pulse shaping is possible for a very broad frequency spectrum from the IR to the UV, due to the transparency range of many molecules in the gas phase. In the experiment, the gas was placed in an optical fibre, a concept that has been used in a range of pulse shaping and compression schemes. A review on nonlinear fibre optics can be found in Agrawal.[57]

2.9 Pulse characterisation

Central to the use of ultrafast laser pulses in chemistry and physics is their characterisation. Without knowledge of the duration, bandwidth and phase structure, in addition to the central wavelength, it is simply not possible to take full advantage of ultrafast pulses. Characterisation of ultrashort laser pulses is a challenging task, as in principle the measurement needs to be performed with a device that has a faster response than the event to be measured. However, there is no faster event than the light pulse itself, and so successful techniques usually involve using the light pulse itself as a detection tool. In an autocorrelation, a replica of the original pulse is generated and is then overlapped with the original pulse both spatially and temporally in a nonlinear medium. The pulse duration is mapped to a spatial width of the resulting correlation signal (which is often the second harmonic) that can then be used to calculate the pulse duration. A review on methods for single-shot characterisation of femtosecond laser pulses can be found in Brun *et al.*[58] The correlation signal is proportional to the product of the intensities $I(t)$ and $I(t-\tau)$ of the two incoming pulses, such that the detector measures the integral $\int I(t)I(t-\tau)dt$, where τ is the delay between the two pulses. The electric field is related to the intensity by $E(t) = I(t)^{1/2}\exp[-i\phi(t)]$, such that $I(t) = |E(t)|^2$. Therefore, the autocorrelation gives information about the temporal electric field of the pulse but not about the phase $\phi(t)$.

A number of schemes have been developed to extract the phase of the pulse; the two most common ones for femtosecond pulses are based on spectrography, which measures the spectrum, and interferometry, which measures the interaction/interference of laser pulses.

Frequency-resolved optical gating (FROG) is a spectrally resolved autocorrelation technique that utilises one well-characterised laser pulse to measure (or gate) the spectrum of another laser pulse as function of delay between the two.[59] The resulting time-frequency measurement can be represented by a graph, also called a FROG trace; an example[60] is shown in Fig. 4. For a transform-limited pulse, the spectrum remains constant over the pulse duration, while a chirp, *i.e.* a change of frequency with time within the laser pulse results in a tilted FROG trace. The intensity and phase of the laser pulse can be retrieved with an algorithm. There are different possible geometries of the two beams, leading to various implementations, such as for example second-harmonic generation FROG and polarisation gating FROG. The FROG technique works well from the infrared to the UV spectrum. Reviews by Trebino can be found in refs. 61,62.

Iaconis and Walmsley[63,64] developed a pulse characterisation technique called spectral phase interferometry for direct electric-field reconstruction (SPIDER) that is based on spectral shearing interferometry. The method has the advantage of not requiring one well-characterised light pulse at the outset. Nonlinear frequency mixing generates a frequency shear in one of two pulses, which are otherwise identical, and the resulting interference between the sheared and non-sheared pulses is spectrally resolved by a spectrometer. The phase of the input pulse can then be reconstructed from the interferogram. The SPIDER technique has been employed widely for the characterisation of infrared laser pulses, although measurements of pulses around 400 nm were performed by Londero and co-workers[65] and 266 nm by Wu and co-workers.[66] Another feature of SPIDER is that it is possible to measure the electric field not only in the temporal but also the spatial domain, yielding a complete description of the field.[67]

SPIDER acquires a one-dimensional array, and the computational reconstruction of the pulse can be performed fast with a non-iterative algorithm, as has been demonstrated by

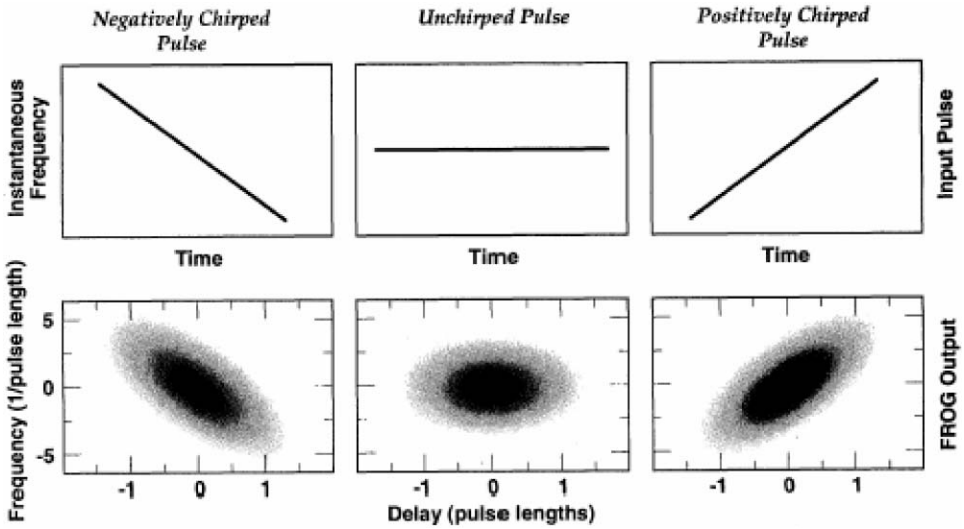

Fig. 4 FROG traces for negatively chirped, unchirped, and positively chirped Gaussian pulses. The figures in the top row show the instantaneous frequency *versus* the delay between the two laser pulses. The figures in the bottom row show the FROG traces as density plots (black indicates high intensity and white indicates low intensity). Adapted from ref. 60, with permission.

Kornelis and co-workers[68] at 1 kHz. The FROG trace is a two-dimensional array from which the pulse is retrieved with an iterative algorithm, which is more computationally intensive. Kane and co-workers developed a real-time FROG that works at 20 Hz.[69]

The increasing application of shaped laser pulses in photochemistry and photophysics is driving the current interest in the development of novel and robust methods for reconstructing the electric field profile of arbitrarily shaped femtosecond light pulses in all regions of the electromagnetic spectrum from the IR to the VUV. A promising method has been demonstrated by Wohlleben and co-workers[70] who used shaped femtosecond laser pulses to excite an atomic two-level system. The resulting coherent transients act as a phase diagram of the laser pulse, such that the phase can be reconstructed. As atomic transitions occur over a very broad spectral range, this method could be used for the characterisation of pulses in that range.

3. Approaches to gas phase samples

A range of techniques are available to generate gas phase samples. Many of these, such as effusion, evaporation, free-jet expansion and laser desorption and ablation, have long histories and will, no doubt, continue to be developed and widely used. Nonetheless as molecular targets for spectroscopy increase in size and complexity, new techniques will be required, and some promising candidates are reviewed below.

3.1 Helium nanodroplets

In what can be seen as a combination of molecular beam and matrix isolation techniques,[71] superfluid helium droplets containing one or more impurity molecules have proven to be extremely exciting spectroscopy tools. Helium droplet techniques have been pioneered by Toennies and co-workers in Göttingen. The droplets are generated by expansion of gaseous or liquid helium through a small nozzle into a vacuum.[72] Which approach is used determines the droplet sizes, which ranges from a few hundred to up to 10^9 atoms.[73] The helium droplets pass through a 'pick-up' cell containing a low density vapour of the target atom or molecule. The droplets, now containing the target molecules, are then laser-excited, which leads to evaporation of helium, and ionised by, for example, electron impact. The ions are detected by mass spectrometry or bolometric detection of helium depletion.

To date, there have been few ultrafast spectroscopic studies of targets in helium droplets. This may be due to difficulties in suitable detection techniques. Laser induced fluorescence has been utilised (see for example[74]) and recently, resonance-enhanced multiphoton ionisation (REMPI) spectroscopy of benzene in helium droplets was reported.[75]

3.2 Electrospray ionisation

One limitation of the helium droplet approach is the need for the target molecules to be vaporised in the pick-up region. This problem can be overcome by electrospray ionisation (ESI), a technique developed for mass spectrometry whereby large molecules can be brought into the gas phase as ions. The use of electrospray in mass spectrometry was pioneered by Fenn and Mann in the 1980s.[76] The ESI process starts with a solution of the target molecule forced down a capillary (typically a hypodermic needle) with a conical tip. The tip is held at a high electrical potential, up to a few kV, which, as the solution emerges, leads to the formation of a fine charged aerosol. Solvent then evaporates from the droplets leading to increased charge density. This continues until the charge repulsion causes a Coulomb explosion, where the droplet breaks up into smaller charged droplets. The cycle continues until all the solvent has evaporated leaving only the highly charged target ion. If the droplets leaving the tip pass through a counter-propagating gas, the evaporation will be faster, leading to more highly charged ions. In the absence of this gas, slower

evaporation leads to ions with higher mass/charge ratio. This is known as soft ionisation, and is the method of choice for large biological molecules. Of course it is not necessarily desirable to study highly charged ions, and reduction of the charge of the ions formed in ESI has recently been demonstrated.[77]

4 Probes for ultrafast chemical dynamics

In the gas phase, laser induced fluorescence (LIF) and resonant multiphoton ionisation (REMPI) have been the mostly extensively employed methods for observing femtosecond dynamics. These approaches have been exploited for a wide range of applications and have undoubtedly been instrumental in furthering our understanding of ultrafast reaction dynamics. Femtosecond LIF and REMPI methods require the probe laser to be resonant with an electronic transition; however, as a photoinitiated chemical process evolves, its electronic wave function also evolves, so these detection techniques tend to be limited to a small reaction window. In this section we concentrate on newer techniques that are beginning to show great promise due to their ability to map out the whole reaction coordinate.

4.1 Femtosecond time-resolved photoelectron spectroscopy

Femtosecond time-resolved photoelectron spectroscopy (TRPES) is a form of pump–probe spectroscopy in which an ultrafast laser pulse creates a non-stationary state, or wave packet, the dynamics of which are then monitored by recording the kinetic energy of electrons generated by ionisation with a second ultrafast laser pulse.[78] The great advantage of TRPES over the more traditional pump–probe techniques is that the probe laser pulse does not need to be resonant with any electronic states in order to ionise the sample. In addition, because the vibrational and electronic structures change along a reaction path, TRPES can monitor molecular dynamics at all points along a reaction coordinate. Crucially, it has been shown that nuclear motion can be effectively decoupled from electronic motion[79] to allow molecular vibrations to be followed. TPRES therefore represents a global probe that is broadly applicable in photochemical reaction dynamics.

Photoelectron spectra are recorded using traditional time-of-flight apparatus, a magnetic bottle spectrometer or imaging detectors. These have all been discussed extensively in the literature and are mentioned only briefly here. In field-free time of flight, photoionised electrons are ejected along the axis of the flight tube of a linear time-of-flight apparatus and detected,[80] usually by a micro-channel plate (MCP). The obvious drawback of this approach is that only very few of the ejected electrons reach the detector, and so the detection efficiency is very low. The magnetic bottle photoelectron spectrometer (MBPES) is a time-of-flight device developed by Kruit and Read[81] specifically to improve the detection efficiency and resolution. The device comprises an interaction region through which a parallel magnetic field passes along the time of flight axis. Away from the interaction region the field diverges and weakens, then becomes parallel again, forming the shape of a wine bottle. All electrons emitted in the hemisphere facing the detector develop a spiral trajectory around the field lines and are directed to the detector. Addition of an electric field in the interaction region ensures that nearly all electrons reach the detector. MBPES has been employed in studies of neutral species,[79] water clusters[82] and has recently been extended to anion photodetachment experiments.[83]

An increasingly popular approach is photoelectron/photoion velocity map imaging, first demonstrated by Chandler and Houston,[84] and improved by Eppink and Parker[85] and Offerhaus *et al.*[86] The spectrometer comprises parallel extractor and repeller plates, a time-of-flight region and a detector, usually a MCP coupled to a phosphor screen and imaging detector such as a charge-coupled device (CCD) camera. In operation, the three-dimensional velocity distribution of electrons ejected by photoionisation is projected onto the detector by an applied electric field, where it forms a series of concentric rings (see Fig. 5A) corresponding to the electron kinetic energy and angular distribution. The power of this approach arises because, if there is an axis of symmetry in the interaction region parallel to the detector, then the original 3D velocity distribution can be regenerated from the image by an inverse Abel transform or iterative procedure.[87]

To date TRPES has been applied to a diverse range of chemical systems, and has been reviewed thoroughly by Stolow, Bragg and Neumark.[78] Recent targets include

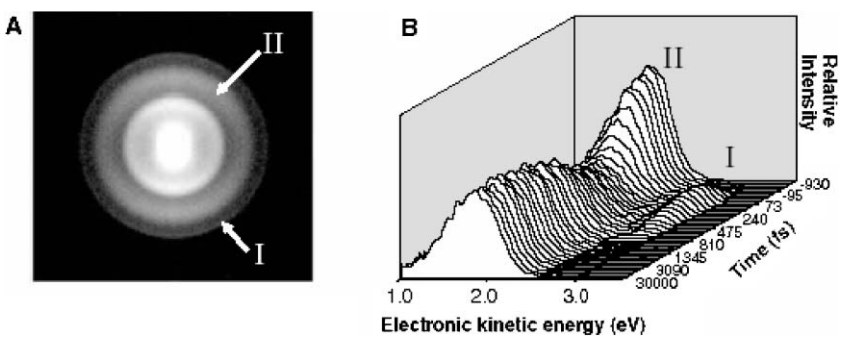

Fig. 5 Femtosecond time-resolved photoelectron spectra of $(D_2O)_{25}^-$. A. Photoelectron image from clusters excited by 100 fs pulses of 1260 nm and probed by 100 fs pulses at 400 nm at one pump–probe delay. Photoelectrons from the ground s state are marked II, and those from the excited p state are marked I. B. Photoelectron spectra extracted from the images for different time delays. Excitation of the cluster at 1260 nm simultaneously depopulates the ground state and populates the excited state. Relaxation to the ground state can be seen to occur on the timescale of approximately 400 fs. Reproduced from ref. 96 with permission.

polyatomic organics, for example, a range of α,β-enones (acrlein, crotonalehyde and methyl vinyl ketone),[88] and electronic relaxation dynamics of isolated DNA and RNA bases.[89] Tsubouchi, Whitaker and Susuki[90] studied singlet–triplet intersystem crossing, and rotational alignment in pyrazine by photoelectron imaging, as well as time-resolved photoelectron angular distributions. Weber *et al.*[91] have studied charge transfer processes in 2-phenylethyl-*N*,*N*-dimethylamine following excitation in either a (1+1) photon excitation at 266 nm or a (2+1) photon excitation at 400 nm. Their experiment monitors changes in photoelectron spectra of the Rydberg states of the molecule. Tsuboushi, de Lange and Suzuki[92] have used time-resolved photoelectron imaging to study ultrafast dissociation of the NO dimer following excitation at 200 to 235 nm.

Femtosecond photoelectron spectroscopy of molecular anions and clusters was pioneered by Neumark's group. In this case the probe laser photodetaches the extra electron and it is detected in a time- and energy resolved experiment. Molecular anions have included I_2^-.[93] Using this technique, Sanov and co-workers were able to map the reaction coordinates of dissociating I_2^- and IBr^-.[94]

Cluster anions, both homo- and heterogeneous, are providing a rich seam of experiments. Bragg *et al.*[95] have used image-derived photoelectron spectra of small mercury cluster ions (Hg_n^-, n = 7–18) to elucidate their electronic relaxation dynamics. The same group[96] has examined the hydration dynamics of an electron, shown in Fig. 5, in negatively charged water clusters of between 50 and 100 molecules. Following excitation by a 1250 nm 100 fs laser pulse, relaxation of the electron was monitored by photodetachment by a 400 nm 100 fs pulse and photoelectron spectroscopy. At the same time Zewail and co-workers[82] studied exactly the same system but excited the electron with an 800 nm pulse. Both studies indicated that the relaxation occurred on the same timescale as bulk water (between 180 fs and 130 fs depending on the cluster size). Other anion cluster studies include homogeneous and heterogeneous solvation dynamics in $[(CO_2)_n(H_2O)_m]^-$ clusters[97] and product branching ratios in the dissociation of iodine from binary cluster anions with Ar, H_2O, CH_3I and CH_3CN.[98] Bernhardt *et al.* have studied intramolecular vibrational relaxation processes in Ag_2Au clusters.[99] In this example, near-zero kinetic energy time-resolved photoelectron spectroscopy was performed on neutral clusters formed by photodetachment from mass-selected ions.

Hayden and co-workers combined femtosecond time-resolved photoelectron–photoion coincidence (PEPICO) spectroscopy with energy and angle-resolved imaging to study multiphoton dissociative ionisation dynamics of NO_2 at 375.3 nm.[100,101] This technique, called coincidence imaging spectroscopy (CIS), has also been applied to photodissociation of the nitric oxide dimer, $(NO)_2$, at 200 nm and 209 nm[88] and the OHF^- ion to elucidate the transition state of the $OH + F \rightarrow O + HF$ reaction.[102]

Single photon ionisation offers the greatest clarity as a probe of molecular dynamics, but for many interesting molecules single-photon ionisation occurs in the vacuum ultraviolet (VUV). VUV photoionisation and photoelectron spectroscopy are well developed high-resolution tools using synchrotron radiation or nonlinear VUV generation from tabletop lasers.[103] Femtosecond VUV sources have been developed[104] using 2-photon resonant difference four-wave frequency mixing to generate femtosecond pulses in the wavelength range 102 nm to 124 nm, and by high-order harmonic generation in a rare gas jet, discussed in section 2.7. Nugent–Glandorf *et al.*[105] used such an instrument to perform a pump–probe experiment to observe the time-resolved dissociation of Br_2. The challenge with these approaches, in addition to low intensity, is wavelength selection. To date there have been few demonstrations of ultrafast VUV or XUV molecular photoelectron spectroscopy.

4.2 Ultrafast electron diffraction

Gas-phase electron diffraction has been developed over the last 20 years (see ref. 106 and references therein). Wilson and co-workers[107] explored ultrafast electron and X-ray diffraction theoretically, and Zewail and co-workers[108] have pioneered picosecond time-resolved electron diffraction experimentally. In this technique the target molecule is excited by an initial laser pulse, but unlike traditional pump–probe spectroscopy, the probe is not a second laser pulse, but a short pulse of electrons. The electron pulse is generated by laser-induced photoemission from a metal cathode by a femtosecond laser pulse. The emitted electrons, numbering only a few thousand to minimise space-charge effects, are accelerated to between 40 keV and 100 keV before impinging on molecules in a gas jet or molecular beam. Electrons scattered by the interaction generate a time-dependent diffraction pattern that is recorded on an on-line imaging detector, such as a CCD camera. Due to the anisotropy of the molecular sample, the diffraction pattern is a series of concentric rings, which can be refined to reveal the structure at each time step. These experiments are currently able to achieve spatial and temporal resolutions of 0.01 Å and 1 ps respectively.

Electron diffraction has three key advantages over X-ray diffraction. The first is that, because electrons scatter both from electron clouds centred on atoms and those located between atoms, the technique is able to interrogate all atoms and atom pairs in the molecule. Secondly, the Coulomb interaction between the electrons gives scattering intensities 5 or 6 orders of magnitude larger than for X-rays. Finally, the availability of femtosecond lasers means that ultrafast electron diffraction can be carried out in the lab, whereas ultrafast X-ray pulses are available only at synchrotrons.

Despite its obvious power, ultrafast electron diffraction has been exploited by few researchers, presumably because of the formidable experimental challenges it presents. Nonetheless, it is starting to appear in the literature[109,110] and the Zewail group have looked at an impressive array of problems. These include elucidating transition state structures occurring in radiationless transitions in the photochemical reaction pathways of pyridine[111] and other heteroaromatics;[112] transient structures in non-concerted reactions in organics[113–115] and organometallics;[116,117] structures of carbene intermediates in the dissociation of diiodomethane;[118,119] pseudorotation of the cyclopentadienyl radical following its dissociation from cyclopentadienyl cobalt dicarbonyl.[120] The complexity of the

targets and reactions is steadily increasing, and now includes non-equilibrium structures in photoinduced ring opening reactions of 1,3,5-cycloheptatriene and 1,3-cyclohexadiene[121] and rearrangement and ring opening of 1,3,5-cyclooctatetraene.

Another approach to electron diffraction has come out of work on attosecond optical pulse generation and was proposed by Zuo, Bandrauk and Corkum.[122] During multiphoton ionisation by an intense ($\sim 10^{14}$ W cm^{-2}), few-cycle laser pulse an electron wave packet is at first pulled away from the ion by the electric field of the light. When the same cycle of the light field reverses direction, the electron is accelerated back to the ion, where it is scattered. Elastic scattering leads to a diffraction image of the parent ion.[123] The technique has been applied theoretically to the H_2^+ model system and is yet to be demonstrated experimentally. However it offers some compelling advantages over other approaches to ultrafast electron diffraction. Because the electron is formed where it is needed and the ionisation is occurring in less than one optical cycle, the spatial and temporal resolution are both very high (1 Å and 1 fs respectively) and the electron flux is very high. On the other hand, so far the technique is limited to diatomic molecules and these are required to be aligned in the laboratory frame.[124] Furthermore the high intensity of the laser modifies the electronic states of the molecule.

A related technique uses the high-order harmonics generated by the electron recollision to make a tomographic *image of the wavefunction* of the highest occupied molecular orbital of a molecule, which has been demonstrated experimentally for N_2.[124] Conceptually this approach is exactly like the diffraction described above, but relies on the sensitivity of the harmonic intensity to the relative orientation of the molecular axis and the laser polarisation. Hopefully this technique, and by extension also diffraction, can be applied to larger, more complex molecules.

5. Coherent control using femtosecond lasers

Having recognised the quantum mechanical nature of matter at the atomic and molecular level, it is inevitable that attempts would be made to manipulate, and if possible fully dictate, the quantum state distribution of such systems. This endeavour has become known as coherent control or quantum control and is a flourishing field.

The high coherence and intensity of laser light has meant that most coherent control efforts have involved their use, although now it is extending to exploit the coherent properties of Bose-Einstein condensates to control reaction dynamics on surfaces, at least in theory.[125] The earliest experiments attempted to utilise the high intensity and monochromacity of laser light to selectively cleave chemical bonds by exciting their vibrational overtones. This was unsuccessful because the energy put into the bond is rapidly redistributed among other vibrational modes of the molecule.

Approaches to coherent control usually fall into either the frequency domain or the time domain, roughly along the lines of the division between narrow band and broad band lasers. Frequency domain coherent control was proposed by Shapiro and Brumer.[126] The central idea is that in order to control the population of a final quantum state, it must be simultaneously accessed by multiple independent excitation paths.[127] The net excitation is a result of interference between the competing pathways, and control is achieved by altering the relative phases and amplitudes of those pathways. There are numerous ways to implement these ideas using combined single photon and multi photon excitations, including $(\omega + \omega + \omega) + 3\omega$, $(\omega + \omega) + 2\omega$ and $(\omega_1 + \omega_2) + (\omega_2 + \omega_1)$, where ω is the photon frequency, and ω_1 and ω_2 are two different frequencies. The first of these is the most frequently discussed[128] and combines one- and three-photon transitions so that the angular momentum selection rules allow both routes to access the same final state. The popularity of this formulation stems from the ease with which it can be implemented by tripling the output of a pulsed narrow band (nanosecond) laser.

A whole series of frequency domain coherent control methodologies fall into the category of adiabatic population transfer, and they are beautifully reviewed by Vitanov *et al.*[129] Adiabatic population transfer can achieve efficiencies very close to 100% for some systems. One powerful variation of this approach is stimulated Raman adiabatic passage (STIRAP) and its derivatives. In STIRAP two lasers are used to couple three states, as shown in Fig. 6, with the objective of transferring population from state |1> to state |3>. It has been found that to achieve high population transfer the two laser pulses have to be timed in a rather surprising way. The Stokes pulse, with frequency ω_{23}, has to be applied before the pump pulse, which has frequency ω_{12}.

Time domain and frequency domain approaches to coherent control are in fact equivalent, as shown by Shapiro and Brumer[130] and in many ways overlap.[131,132] In this review however we will confine our attention to time domain control schemes that employ ultrafast lasers. Different control schemes are considered from the point-of-view of the phase complexity of the laser fields used, as this largely reflects their historical development.

5.1 Phase-locked laser pulses

The first experiments in, and theoretical treatment of short pulse excitation were pump–probe and pump–dump schemes. A short laser (pump) pulse excites a coherent superposition of stationary states of the system–a wave packet. Although

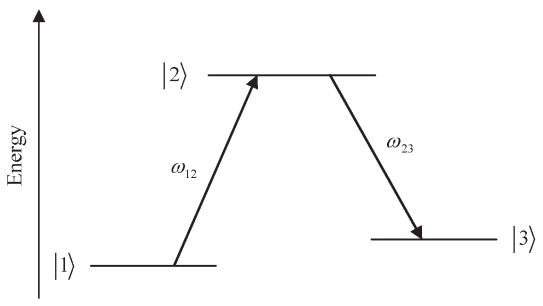

Fig. 6 Schematic representation of STIRAP for an ideal three level system sometimes referred to as a Λ-atom. The laser fields, ω_{12} (the pump pulse) and ω_{23} (the Stokes pulse), lead to time dependent mixing of the stationary states |1>, |2> and |3>. Population is transferred from state |1> to state |3> without ever populating state |2>.

coherent, and therefore phase synchronised, this work was not primarily concerned with phase evolution. The stationary states can be rotational, vibrational or electronic, or combinations of them. The excitation is impulsive–the duration of the excitation is short compared to the timescale of the wave packet evolution. The wave packet evolves in time and its behaviour can be monitored by a second, time delayed short laser pulse, called the probe. Pump–probe investigation of wave packet dynamics continues to be applied to increasing complex systems.[133]

The first control experiments and theory developed from this idea. Instead of simply monitoring wave packet evolution, in some systems controlling the timing of the second pulse can select between two or more final states. The classic demonstration of this approach was made by Gerber and co-workers[134] in the sodium dimer, the excitation scheme for which is shown in Fig. 7. From the Na_2 X $^1\Sigma_g^+$ ($v'' = 10$) ground state, a one photon excitation with a 70 fs laser pulse at 627 nm created a vibrational wave packet in the A $^1\Sigma_u^+$ ($v' = 10$–14) state of with a period of 306 fs. Simultaneously, a two photon excitation formed a wave packet in the 2 $^1\Pi_g$ ($v' = 11$–18) state which has a period of 363 fs. A time-delayed but otherwise identical laser pulse was used to probe the wave packet motion. Two-photon ionisation by the probe laser from the inner turning point of the A state wave packet generated the $^2\Sigma_g^+$ state of the Na_2^+ ion. From the outer turning point of the 2 $^1\Pi_g$ wave packet the probe laser made a single photon excitation to a doubly excited Rydberg state, which autoionised to Na_2^+ ($^2\Sigma_g^+$), and dissociated to give Na^+ and Na(3s).

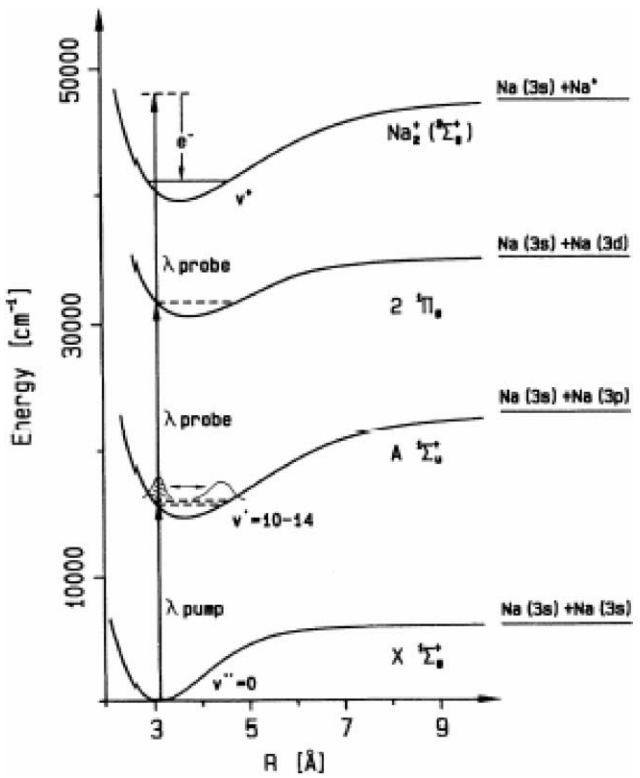

Fig. 7 Coherent control scheme in the sodium dimer. A 70 fs laser pulse at 627 nm simultaneously created wave packets in the A $^1\Sigma_u^+$ potential and the 2 $^1\Pi_g$ potential by one and two photon excitation respectively. Time delayed ionisation from these wave packets by respectively two and one photon excitation, again at 627 nm, lead to a time-dependence in the photoelectron kinetic energy. Reproduced from ref. 134, with permission.

The related pump–dump approach was formalised by Tannor, Kosloff and Rice.[135,136] Their model is based on a ground state potential energy surface of a molecule ABC featuring a minimum separated from two product channels, say AB + C and A + BC, by saddle points. Above the ground state surface is an excited state surface with a minimum that is displaced from that of the ground state, and has rotated normal coordinates. An ultrafast (femtosecond) laser pulse excites vertically from the ground state, forming a vibrational wave packet on the excited surface. The wave packet evolves on the excited state surface and at some later time is pumped back down to the ground state surface by a second ultrafast laser pulse. If the wave packet on the excited surface takes the molecule to geometries corresponding to those in the product channels of the ground state, vertical transitions from these points will place the wave packet in a product channel of the ground state. The second laser pulse can be timed, therefore, so that it causes de-excitation into products.

Pulse sequence experiments, in which the time delay and relative phase between two laser pulses are varied, were initially used to study wave packet evolution. Fig. 8 shows the relationship between the coarse time delay between two ultrafast laser pulses and the phases of their electric fields. The phase of the second pulse is considered relative to the phase of a notional carrier frequency, ω_0, which is set to the phase of the first pulse. Experimentally the phase shift is achieved by a tiny time delay. Zewail and co-workers performed the first experiments in iodine[137] and anthracene,[138] controlling the relative pulse phase and delay with an acousto-optic modulator. Scherer *et al.*[139] measured fluorescence to follow the temporal behaviour of rovibrational wave packets in iodine vapour generated by phase-locked pulse pairs from Michelson and Mach-Zender interferometers. That work led to the first demonstration of control by the same group.[140] The total excited state population of the iodine molecule was

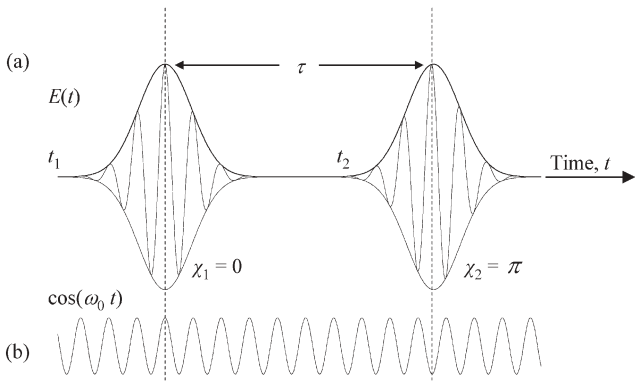

Fig. 8 A cartoon illustrating the phase relationship between two time delayed laser pulses. (a) The two pulse envelopes are separated by time τ. The electric fields of the pulses oscillate beneath the envelopes. The electric field of the first pulse, at time t_1, is exactly in phase with the notional carrier frequency, ω_0, shown in (b), whereas the pulse at time t_2 is exactly out of phase with the carrier.

monitored by fluorescence as a function of the phase difference between the two pulses for a fixed time delay.

Noel and Stroud[141] proposed and executed a coherent control scheme in the Rydberg states of potassium. They excited two identical time-delayed phase-locked wave packets centred around principal quantum number $n = 66$ with a 15 cm^{-1} bandwidth (picosecond) laser. Fig. 9 is a cartoon illustrating the dynamics of such a wave packet. Formed in the vicinity of the nucleus the wave packet makes several Kepler (or classical) orbits before dispersing and rephasing into several partial revivals, eventually reforming the original wave packet once again. In this experiment, shown schematically in Fig. 10, the second wave packet was excited after a delay of half the classical orbit period. The system was then allowed to evolve until the second order partial revival, at which time each wave packet has split into two little wave packets. This ensured that the two initial wave packets overlapped spatially and could therefore interfere. The phase of the second wave packet determined the outcome of the interference. Three key phase differences were identified. If the phase was $\pi/2$ the interference completely removed the fractional wave packet at the outer turning point at the time of the second order partial revival. If the phase was $-\pi/2$ the fractional wave packet at the inner turning point was destroyed. A phase difference of π left both fractional wave packets intact but shifted their phases. Removing one fractional wave packet effectively shifts the time of the full revival.

Fielding and co-workers employed wave packet interference to exploit *accumulated* phase relationships between constituents of Rydberg wave packets in atoms and molecules. The experiments manipulated the electronic angular momentum in xenon atoms,[142] sodium atoms,[143] the ratio of predissociation to autoionisation in NO,[144] and rotational angular momentum in NO.[145] The xenon and sodium work exploited the phase shift that arises as a result of the different quantum defects of the Rydberg series comprising the wave packet. As the wave packet orbits this phase difference increases. By exciting a second wave packet, phase matched to the first, one or other angular component (*s* or *d*) could be selectively enhanced or diminished. In the NO rotation control experiments, a phase contribution from the different rotational series of a Rydberg wave packet was utilised in a similar way. In this case it was possible to create, from an initial superposition of both, a wave packet comprising only $N^+ = 0$ or $N^+ = 2$, where N^+ is the rotational quantum number of the core.

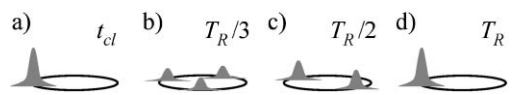

Fig. 9 A cartoon showing the temporal evolution of a radial Rydberg electronic wave packet. a) A wave packet formed near the nucleus (at the leftmost end of the orbit) will undergo several 'classical' orbits, each taking time $t_{cl} = 2\pi n^3$, where n is the average principal quantum number of the wave packet. At later times the wave packet disperses and rephases. Eventually, at the revival time given by $T_{rev} = nt_{cl}/3$, the original wave packet reforms, d). At intermediate times given by $T_N = T_{rev}/N$, the rephasing forms sub wave packets or partial revivals, where N is the order of the partial revival and the number of sub wave packets, b) and c).

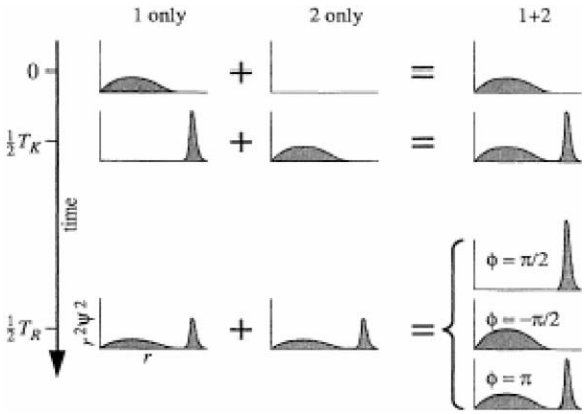

Fig. 10 Cartoon plots of the radial distribution function at key times in Rydberg wave packet coherent control experiment of Noel and Stroud (ref. 141). Columns 1 and 2 shows the behaviour of two isolated single wave packets. Column 3 shows the result of the coherent sum of the two wave packets in a single atom. The bottom row shows the phase-dependent effect of interference between the wavepackets at the time of the second order partial revival. A phase difference of $\phi = \pi/2$ between the first and second wave packets removes one sub wave packet, whereas $\phi = -\pi/2$ removes the other. $\phi = \pi$ has no net effect on the wave packet. Reproduced with permission.

Girard *et al.*[146] have used phase-shifted transform-limited pulses to control interference between matter wave packets in Na^+ formed by predissociation from NaI. Suitably phased pulses could be used to control the kinetic energy of the fragments. Free particle wave packet interference was also demonstrated for electrons ionised from potassium.[147] A pair of time-delayed 30 fs pulses ionised potassium from the 5*p* state. Two ionisation pathways occurred: one-photon threshold ionisation, and two-photon continuum ionisation. The two pathways interfered, depending on the delay between the ionisation pulses, allowing manipulation of the electron wave packet dynamics.

Control over bound–bound and bound–free transitions (but not their branching ratios) was reported in NO by Faucher *et al.*[148] using phase-locked non-transform-limited pulses. A two-photon excitation from the ground state to an intermediate (A) state and from there ionised with another two photons. Oscillations were observed in the ion yield as a function of delay between various combinations of intermediate and ionisation steps.

5.2 Chirped-pulse coherent control

The next step in increasing phase complexity brings us to frequency chirped laser pulses. In a chirped laser pulse there is a change of phase with frequency or, equivalently, a change in wavelength with time. Thus the instantaneous frequency of an up- (or positively) chirped pulse increases as the pulse passes, *i.e.* it becomes bluer, whereas that of a down- (or negatively) chirped pulse decreases, *i.e.* it becomes redder. The simplest case of chirping is linear, characterised by a quadratic phase shift, followed by increasingly higher orders, *e.g.* cubic and so on (section 2.4). Most work in coherent control has employed

linear chirp but cubic phase shifts have been considered recently.[149] Chirped pulses will doubtless continue to play an important role in coherent control since they are the simplest shaped pulses and are relatively easy to understand. Likewise, as our understanding of coherent control mechanisms advances, it seems likely that higher order dispersion will turn out to be useful tools.

Single chirped pulses have been used extensively to manipulate quantum state amplitudes and are often combined with a transform-limited probe pulse. A simplification of STIRAP replaces the pair of nanosecond pulses with a single chirped ultrafast pulse for population transfer in a three-level Λ-atom[150] (see Fig. 6). Warren *et al.*[151] used a chirped picosecond laser pulse to selectively excite the transitions $^2P_{3/2} \leftarrow {}^2S_{1/2}$ or $^2P_{1/2} \leftarrow {}^2S_{1/2}$ in atomic sodium–a quasi three-level system. A positive chirp preferentially excited $^2P_{1/2}$ whereas a negative chirp only excited $^2P_{3/2}$. The same group has also extended this approach to I_2, a multi-level system.[152,153] Chelkowski *et al.* proposed a vibrational ladder-climbing approach to dissociate H_2[154] using a chirped pulse. Vibrational levels are sequentially excited as the negatively chirped pulse comes into resonance with the decreasing vibrational transition energies. Eventually the asymptotic levels are reached and the molecule dissociates. Their view was that this approach should be applicable to polyatomics provided the pulse was short compared to the vibrational relaxation time.

Experimentally, vibrational ladder-climbing has been demonstrated in the $X\,^2\Pi_{1/2}$ state of NO[155] where the excitation $v'' = 0 \rightarrow v' = 1 \rightarrow v = 2$ led to enhanced $v = 2$ population when the chirp follows the reduction in vibrational energy levels. A chirp dependent oscillation in the population was also observed due to interferences between different rotational pathways in the excitation. Electronic ladder climbing has been seen in $5s \rightarrow 5p \rightarrow 5d$ excitation of atomic rubidium by a chirped pulse,[156] and is shown in Fig. 11. The "intuitive" case, where the chirped pulse comes into resonance first with the $5s \rightarrow 5p$ transition followed by the $5p \rightarrow 5d$ transition, leads to complete population inversion. Surprisingly the "counter intuitive" case, where the resonances are reversed, works equally well, at least when the laser intensity is high. Gerber *et al.*[157] found that in Na_2, multiphoton excitation by a negatively chirped pulse led to enhanced final state population compared with a positively chirped pulse, but the positively chirped pulse gave a higher Na^+ yield upon multiphoton ionisation. The group of Girard has studied several systems using single chirped pulses. In the two-level system formed by the $5p \leftarrow 5s$ transition of atomic rubidium excited by a weak chirped pulse,[158] chirp dependent oscillations occur in the population of the excited state. These resulted from interference between resonant and non-resonant excitation pathways and occurred only after the pulse passed through resonance. Similar results were reported for multiphoton excitation of Na[149] leading to enhancement of the final population compared to excitation with a transform-limited pulse. Using interference between wave packets in the $4\ ^2P_{1/2}$ and $4\ ^2P_{3/2}$ states of potassium formed by a chirped pulse and a transform-limited pulse,[159] the same group was able to shape the wave packets and alter their dynamics.

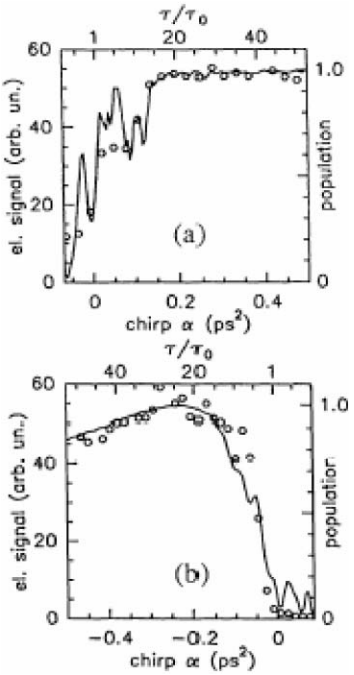

Fig. 11 Results from an electronic ladder climbing experiment in atomic Rb vapour excited by a chirped laser pulse. Positive chirps (red to blue sweep) of $\alpha > 0.2$ ps^2 lead to complete population transfer from the ground 5*s* to the excited 5*d* state. Pulses with a negative chirp also achieved complete population inversion when the chirp was $\alpha = -0.2$ ps^2 . Reproduced from ref. 156 with permission.

Bardeen *et al.* demonstrated a pump-dump experiment to control vibrational and electronic population in the laser dyes LDS690 and LDS750[160] and bacteriorhodopsin[161] in solution using excitation by a single chirped pulse. A similar approach was used in 3-3′-diethylthiatricarbocyanine iodide (DTTCI) in ethanol.[162] Fig. 12 shows schematically how a vibrational wave packet is formed on the excited state potential energy surface by the blue leading edge of the chirped pulse. The wave packet moves to the outer turning point of the potential and, in a stimulated emission process, is pumped back down to the ground state potential surface by the trailing red edge of the pulse. These are solution phase experiments, but the mechanism bears a strong resemblance to the work of Neumark and Zewail in water clusters discussed previously, so it seems likely that theses chirped pulse schemes could be used in clusters. Other studies also take the perspective of wave packet motion. Wilson *et al.* studied vibrational wave packets in the B-state of I_2 in the gas[163] and condensed (in solid Kr)[164] phases. The same group also revisited an early Zewail coherent control experiment in NaI.[165] They found that a chirped pulse could pre-compensate for dispersion of the wave packet over its trajectory in such a way that it was 'focused' into an optimal Franck–Condon window for subsequent excitation. This approach, shown in Fig. 13, increased the yield of excited state sodium atoms from excitation of NaI and the ionisation yield from excitation of I_2.

Multiple chirped pulses. Warren and Davis[166] considered theoretically a Raman chirped adiabatic passage scheme using

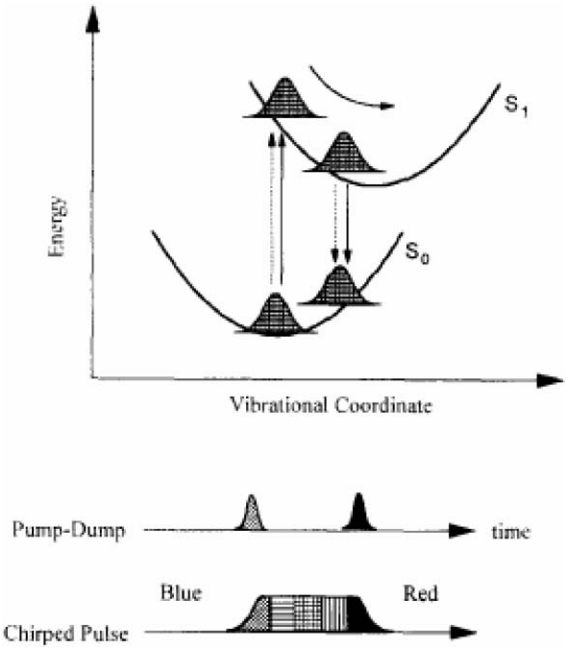

Fig. 12 Schematic representation of the single chirped pulse pump-dump coherent control scheme for large solution phase molecules. The blue edge of the chirped laser pulse (bottom) excites a vibrational wave packet on the upper surface. The wave packet quickly relaxes (curved arrow) and is then pumped down to the ground state again by the red end of the laser pulse. This excitation is equivalent to excitation by two time-delayed pulses where the second pulse has a longer wavelength. Reproduced with permission from ref. 160

two chirped pulses. This allows selective population of ground-state vibrational levels. Sen *et al.*[167] extended these ideas theoretically to two oppositely chirped pulses making a non-resonant stimulated Raman excitation of H_2 from $v'' = 0, J'' = 0$ to $v' = 1, J'$. A negatively chirped pump pulse combined with a positively chirped Stokes pulse placed all the population in the S-branch if the pulse was long and the chirp slow. Reversing the chirps of the pump and Stokes pulses populates only the Q-branch. If the pulse is short and the chirp is fast, then the S/Q branching ratio can be controlled by the chirp. Sauerbrey *et al.*[168] created a very simple technique to selectively excite one or other of the 5 $^2P_{1/2}$ and 5 $^2P_{3/2}$ states of rubidium, which is shown schematically in Fig. 14. Interference between two phase-locked chirped pulses leads to modulation of the frequency spectrum of the pulse pair. The positions of peaks and troughs in the spectrum can be controlled simply by phase shifting two replicas of the chirped pulse with a Michelson interferometer. Selective excitation was achieved by placing a spectral hole at one resonant frequency and a peak at the other.

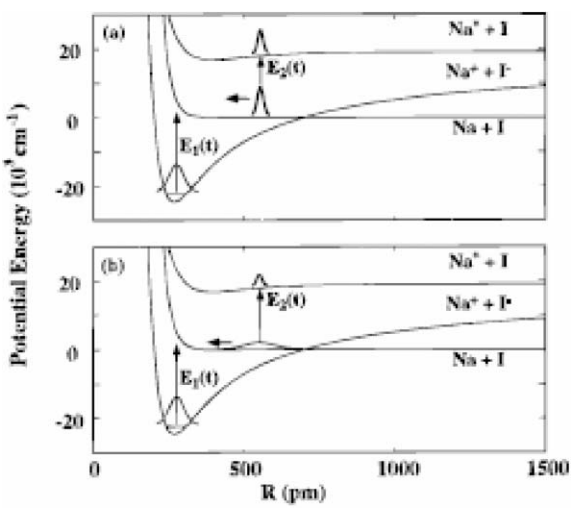

Fig. 13 Schematic of the effect of chirped pulses on vibrational wave packets in NaI. The upper trace shows how a negatively chirped pulse localises the wave packet at the outer turning point of the intermediate potential energy well, from where it can be efficiently excited on to the Na*I potential. A positive chirp disperses the wave packet at the outer turning point (lower trace), leading to less efficient transfer to the excited state. Reproduced with permission from ref. 165.

Additional theoretical proposals for the use of multiple chirped pulses include chirped adiabatic passage by two-photon absorption (CAPTA).[169] This allows selective excitation of *single* rovibrational states of a diatomic by non-resonant excitation *via* an electronic intermediate. Very recently Dunning and co-workers[170] proposed an extension of the half-cycle pulse control of Rydberg electron wave packets to include trains of chirped pulses that, modulated in the right way, control the dynamics of the wave packet.

It is not clear why there have been relatively few coherent control schemes involving two or more chirped pulses, aside from experimental difficulties, which are surely less than for more complex pulses. The authors hope that the future will see this shortfall rectified.

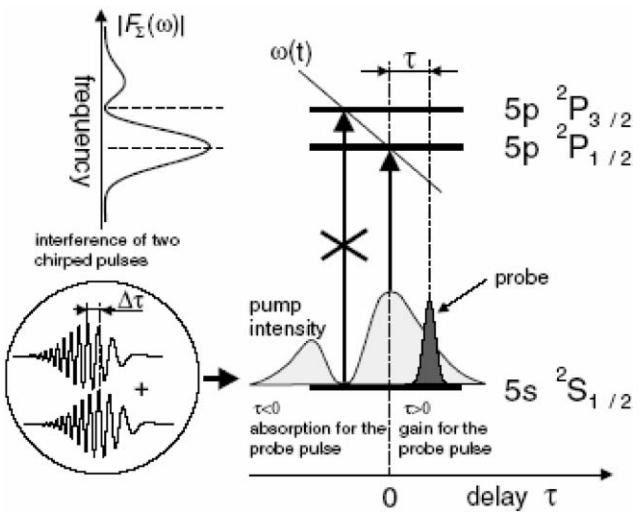

Fig. 14 Selective excitation of Rb atoms by two chirped pulses. Interference between two identical but time-delayed chirped pulses (shown in the inset circle) modulates the frequency spectrum (upper left of figure). By changing the pulse delay, the modulation can be arranged so that an intensity 'hole' lies at the frequency of one transition (corresponding to excitation of the $^2P_{3/2}$ state) and an intensity maximum lies at the other transition frequency (in this case, excitation of the $^2P_{1/2}$ state). Reproduced from ref. 168 with permission.

5.3 Pulse shaping in coherent control

The advent of programmable pulse shaping of ultrafast laser pulses with the techniques described in section 2.8 has made it possible to generate laser pulses with regular phase functions that are much more complex than linear chirp, as well as essentially arbitrary phases and amplitudes. This section starts with a description of some coherent control experiments which have employed regular phase functions, such as phase steps,[171–173] sine functions[171] and square waves,[174] and then moves on to arbitrary phases output by feedback-based optimisation.

Regular phase functions. The application of regular phase and amplitude functions to pulse shapers leads to shaped pulses that can be more readily understood than those formed in feedback control and machine learning (see next section). For example, application of a sine phase function to an SLM pulse shaper generates, from a single input pulse, a train of pulses in the time domain. In our view this approach will take a central role in our understanding of coherent control mechanisms, as the shaped pulses can perhaps be related to fundamental spectral properties of the molecules being excited, for example a wave packet round-trip time.

Meshulach and Silberberg[173,175] demonstrated coherent control of the two-photon transition $8S_{1/2} \leftarrow 6S_{1/2}$ in atomic Cs using a 30 fs laser pulse with a π phase step. The π-step is generated by having the phases $\varphi = 0$ for all frequencies $\omega < \omega_\pi$, and $\varphi = \pi$ for $\omega \geqslant \omega_\pi$, and leads to a "double half pulse",[171] which behaves as a "dark pulse" for $\omega_\pi \approx \omega_{8S \leftarrow 6S}/2$, *i.e.* near the two-photon resonance no excitation occurs, whereas for $\omega_\pi \approx \omega_{8S \leftarrow 6S}/2$ the 8S population is maximal, as shown in Fig. 15, as if excited by a transform-limited pulse. The same approach was found to be applicable also in the laser dye Coumarin 6H, in which the absorption forms a broad continuum as opposed to discrete atomic levels. The Silberberg experiment was repeated in sodium by Baumert and co-workers[171] and extended by the addition of a transform-limited "pre-pulse". By exciting the system first with a phase-locked transform-limited pulse the effect of the π-step pulse could be controlled, and even inverted, depending on the relative phases.

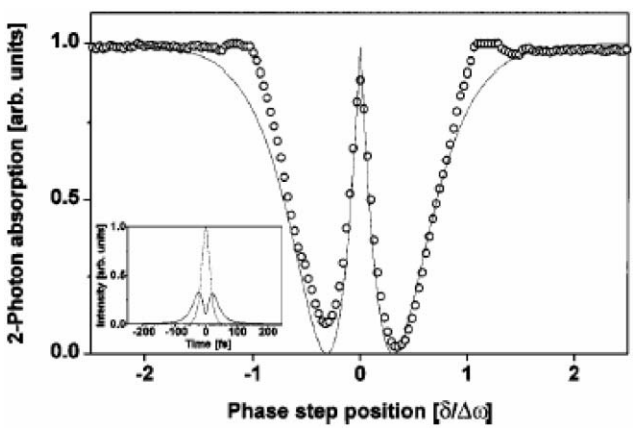

Fig. 15 Experimental (circles) and calculated results (solid lines) for two-photon transitions in Cs gas excited by a pulse with a spectral phase step, as a function of the detuning of the step position from resonance. When the phase step is just above or just below the transition resonance frequency, the shaped pulse makes no excitation. When the step is at the resonant frequency the shaped pulse behaves like a transform-limited pulse, giving maximum excitation. Inset is the calculated temporal intensity of the shaped pulse (solid line) compared to a transform-limited pulse (dashed) with the same power spectrum. Reproduced from ref. 173 with permission.

Meshulach and Silberberg[175] used a cosine phase function to shape 31 fs pulses at 822 nm to generate dark pulses in the same transition in Cs as their π-step work. Motzkus and co-workers[176] also generated dark pulses in a two-photon excitation of atomic sodium using a cosine phase function, but combined it with a feedback algorithm (discussed below). A cosine function applied to the spectral phase of the laser pulse was studied in detail by the Baumert group.[171] A single pulse shaped by a sine phase function generates a train of pulses. The relative phases between the pulses can be controlled by the phase of the sine function. For the two-photon excitation of atomic sodium ($4s \leftarrow 3s$), changing the phase of the function led to enhancement or reduction of the $4s$ population. If the shaped pulse was preceded by a transform-limited pulse, the role of the shaped pulse could itself be controlled, depending on the relative phases between them. Pastirk *et al.*[177] were able to select single fluorescent marker species for excitation in solution mixture by applying a cosine phase function in femtosecond two-photon microscopy.

A square-step phase function was employed by Renard *et al.*[174] to shape 100 fs pulses to control ground state rotational wave packet dynamics in N_2 in a stimulated Raman process. Altering the spectral phase reduced or accentuated interference between contributions from odd and even rotational states.

Perhaps the most sophisticated pulse shaping experiment not to include experimental feedback (discussed in the following section) was performed by the Bucksbaum group.[178] A Rydberg wave packet was excited in atomic caesium by a shaped optical pulse. The initial wave packet included the states $24p$ to $29p$, the population of which was redistributed by a shaped THz half-cycle pulse to include only the $27s$ state.

Irregular phases and genetic algorithms in coherent control. The real power of ultrafast optical pulse shaping has come from its combination with feedback optimisation. In this arrangement, first suggested by Judson and Rabitz,[179] a genetic algorithm (GA) or other automatic optimisation algorithm optimises the shape of the laser field using feedback from the experiment to select a particular objective. The objective can be any of the usual coherent control products, for instance, ionisation yield, particular dissociation products or harmonic generation. A schematic representation of this type of experiment is shown in Fig. 16. This section reviews some examples of coherent control using pulse shaping coupled with genetic algorithms.

The GA combined with a pulse-shaper was first realised by Gerber *et al.* in 1997. In a proof-of-principle experiment, second harmonic generation in a BBO crystal[180] was optimised by correcting a pre-chirped 60 fs laser pulse. The first molecular coherent control was reported by Bardeen and

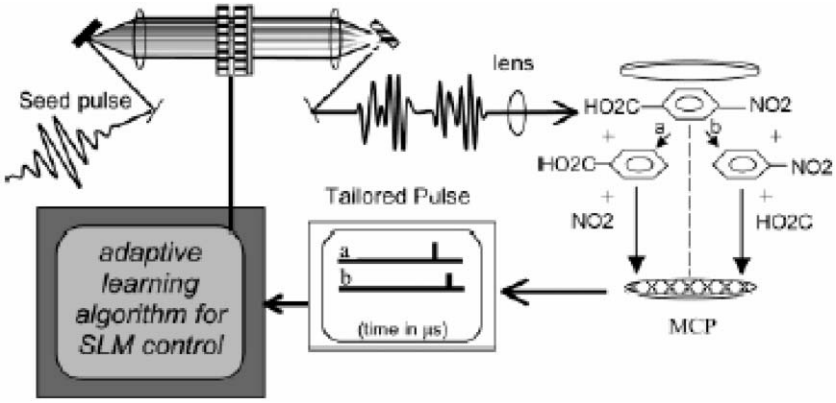

Fig. 16 Schematic representation of a closed-loop pulse-shaping coherent control experiment. Laser excitation leads to photoionisation and photofragmentation. Photoions with different masses are discriminated by their time-of-flight. The genetic algorithm can be programmed to maximise one ion yield over another, for example. The algorithm controls the pulse shaper, forming a range of different shaped laser pulses. The most successful pulse shapes are then used to generate ever more precise selection, all without any input by the user. An optimal pulse is generally found in a few tens of cycles of the closed loop. Reproduced with permission from ref. 201.

co-workers.[181] Their experiment monitored population of the first excited state of the laser dye IR125 in methanol, and demonstrated maximisation of both the efficiency (excited state population/laser power) and efficacy (total excited state population) using feedback from fluorescence. Since that time there have been many studies using these techniques to control excitation of atoms and molecules ranging from dimers to biological macromolecules in gas and solution phases, and even *in vivo* in principle. In atomic physics the GA and pulse shaping approach has selected a particular harmonic (the 27th) from its neighbours in high-harmonic coherent XUV generation in argon in a 175 μm diameter capillary waveguide.[182] More recently, resonant two-photon absorption was maximised in rubidium atoms.[183] In diatomics, Pearson *et al.* were able to select the relative ratios of dissociative ionisation and non-dissociative ionisation in Na_2.[184] Bartelt *et al*. maximised single pulse multiphoton ionisation in NaK (and Na_2K).[185] In Li_2, Leone and co-workers[186] optimised the delay between a shaped pump and a transform-limited probe to maximise the photoionisation yield. The Motzkus group selected arbitrary vibrational states in the potassium dimer by stimulated Raman scattering in a degenerate four-wave mixing experiment.[187] A recent development from the established techniques of phase and amplitude shaping by Brixner *et al.*[203] enhanced the three-photon K_2^+ signal by incorporating polarisation shaping with phase shaping.

Work on polyatomic molecules has included control of the self-phase modulation spectrum of CCl_4,[188] selection of individual vibrational modes in methanol[184,189] and benzene,[184] SF_6 and CO_2,[190] and polydiacetalene.[191] Selective bond cleavage was first demonstrated in $CpFe(CO)_2Cl$ and $Fe(CO)_5$ by Gerber's group,[192] and has now been extended to include fragmentation of CH_3COCF_3[193] and $CpMn(CO)_3$.[194] Fig. 17 shows the experimental results for controlling the photochemical reaction pathway (bond cleavage) for the $CpFe(CO)_2Cl$ experiment, both in terms of the degree of selectivity between reaction products and the optimised laser pulses. Levis and co-workers[195] used pulse-shaping coupled to a learning algorithm in an impressive set of high field experiments in simple organic molecules. Working in the high field, they argued, offers more powerful control over chemical reactions, as it allows ac-Stark shifting of energy levels and multiphoton ionisation, which overcome the limitations imposed by the laser bandwidth in weak field experiments. They were able to selectively enhance photofragmentation products from acetone, trifluoroacetone and acetophenone. In addition the dissociative rearrangement product of acetophenone could be optimised. Other studies in polyatomics include simultaneous optimisation of absorption by solution phase DCM and $[Ru(dpb)_3](PF_6)_2$,[196] and multiphoton excitation of $[Ru(dpb)_3](PF_6)_2$.[197]

Extending both the molecular size and the utility of coherent control, Motzkus *et al.* have studied energy flow in a bacterial light harvesting complex[198] in solution. The complex, its molecular subunits and energy pathways are shown in Fig. 18. The researchers were able to select between intra- and

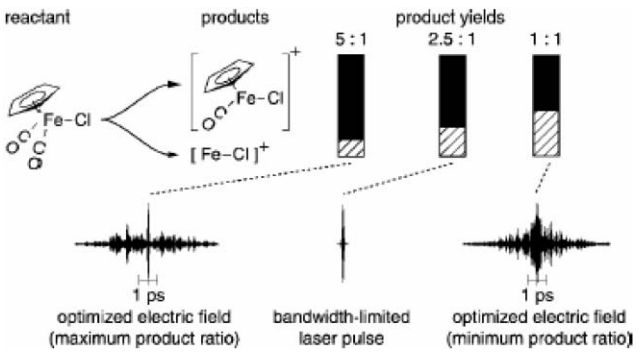

Fig. 17 Feedback optimisation of photodissociation of $CpFe(CO)_2Cl$, where Cp is C_5H_5. The parameter being optimised was the relative yield of $CpFeCOCl^+$ and $FeCl^+$ ions following photoexcitation by pulses shaped by a genetic algorithm. The relative yields are shown by the graphs (top right). $CpFeCOCl^+$ yield is indicated by the dark regions and the $FeCl^+$ by the shaded regions. The pulse shape leading to maximum $CpFeCOCl^+$ yield (bottom left) or maximum $FeCl^+$ yield are shown and compared to the relative yield from a transform-limited laser pulse. Reproduced from ref. 2, with permission.

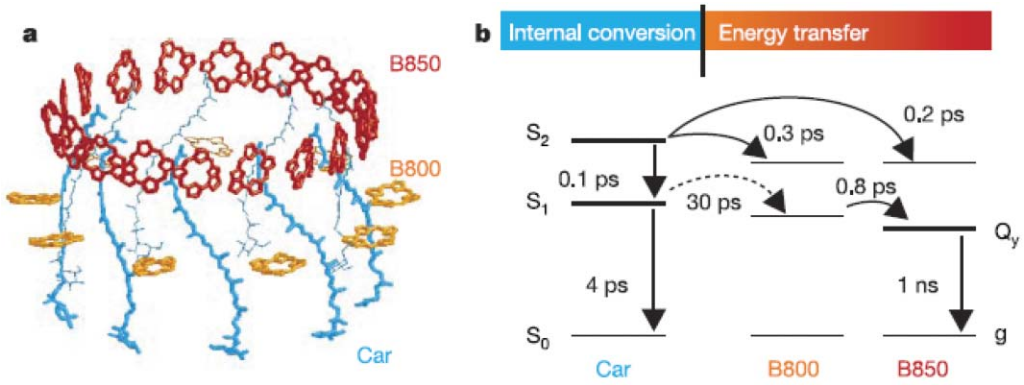

Fig. 18 a) Structure of the light harvesting complex LH2 of the photosynthetic purple bacterium *Rhodopsuedomonas acidophila* showing its carotenoid (Car) and bacteriochlorophyll (bchl) subunits. The bacteriochlorophyll is found in two binding sites, labelled by their absorption maxima, B800 and B850. b) Schematic energy level diagram indicating timescales for internal conversion (IC) and energy transfer (ET) pathways. A closed-loop pulse shaping experiment was able to increase the ratio IC/ET from 1, for excitation by an unshaped transform-limited pulse, to approximately 1.4. Reproduced with permission from ref. 198

intermolecular pathways using shaped ultrafast laser pulses optimised by a closed-loop learning algorithm. The Dantus group has demonstrated that, in principle, coherent control could be used as a probe *in vivo*.[199]

While the experiments discussed above have been enormously successful in achieving control in a wide range of atomic and molecular systems, the complex pulse shapes derived from feedback optimisation have proved difficult to analyse, and have offered relatively little insight into the mechanisms of control. It is no surprise therefore that many in the coherent control community are involved in projects aimed at elucidating those mechanisms. Analysis of a wide variety of experimental results has revealed that the optimally shaped pulses often, but not exclusively, form a pulse train of two or more transform-limited pulses that can be understood in terms of wave packet motion in the system. In some cases these pulses are phase-locked and in some cases not.

The other approach to understanding optimisation experiments is to examine the genetic algorithm for information about the optimal pulses it generates. The Bucksbaum group[200] has pioneered the approach of looking for pulse features that are retained, as the genetic algorithm converges on the optimal pulse, and also for features that appear repeatedly in optimal pulses from several runs of the experiment.

6. Outlook

Femtosecond lasers have had a huge impact on the field of molecular dynamics during the last two decades by providing a light source with the same timescale as molecular vibrations. In order to understand the way in which the motion of *electrons* influences chemical dynamics it is necessary to have a light source with the same timescale as the electronic motion, *i.e.* the attosecond timescale. Attosecond light sources are now a reality, and although applications so far have been in the field of atomic physics, as the technology improves, these new light sources will undoubtedly be exploited to probe electronic dynamics, in real chemical problems. These new attosecond sources will of course also widen the observation window for vibrational dynamics and provide a possible tool for the real time probing of the photodissociation of lighter molecules, such as the model hydrogen halides. There is an increasing interest in the use of time-resolved photoelectron spectroscopy (TRPES) as a probe of ultrafast dynamics and one can imagine the wealth of new opportunities that would be obtained by coupling TRPES with sub-femtosecond VUV light sources. One of the limitations of "conventional" ultraviolet pump and ultraviolet probe TRPES is that the observation window is restricted to the excited potential surface. A VUV probe would provide access to the electronic ground state which is important because the dynamics of polyatomic molecules are heavily influenced by non-adiabatic coupling of vibrational and electronic degrees of freedom and the existence of conical intersections connecting excited electronic states to lower lying electronic states including the ground state. New gas-phase sources such as electrospray ionisation and helium nanodroplets provide us with the opportunity of applying the new femtosecond laser technology to investigate the ultrafast dynamics of increasingly complex systems, such as large biomolecules.

The development of sophisticated femtosecond pulse shaping techniques has revolutionalised the field of coherent control during the last few years. We now have the right experimental tools at our disposal to manipulate the dynamics of quite complex molecular systems. Despite the technological advances, the field is in its infancy and we still have a great deal to learn in terms of understanding why the optimised laser pulses control processes in the way that they do. Unravelling the control mechanisms and developing the rules for predicting the shape of laser pulse needed to control molecular dynamics is a major challenge and one of the driving forces behind the ongoing research in this field. Another important issue is the degree of control which, with the exception of STIRAP, has so far been somewhat limited.

There is absolutely no doubt that the next few years will see exciting new applications of femtosecond lasers in gas phase chemistry.

Acknowledgements

We are grateful to the EPSRC for funding. The authors would also like to thank R. Patel, N. A. Jones, D. S. N. Parker and C. Glendinning for useful comments during the preparation of the manuscript.

References

1 A. H. Zewail, *Angew. Chem. Int. Ed.*, 2000, **39**, 2587–2631.
2 T. Brixner and G. Gerber, *ChemPhysChem*, 2003, **4**, 418–438.
3 M. Dantus and V. V. Lozovoy, *Chem. Rev.*, 2004, **104**, 1813–1859.
4 *Ultrashort laser pulses: generation and applications*, ed. W. Kaiser and D. H. Auston, Springer, Berlin, 2nd edn, 1993.
5 P. M. W. French, *Rep. Prog. Phys.*, 1995, **58**, 169–262.
6 J.-C. Diels and W. Rudolph, *Ultrashort Laser Pulse Phenomena: Fundamentals, Techniques, and Applications on a Femtosecond Time Scale*, ed. P. F. Liao and P. Kelley, Academic Press, San Diego, 1996.
7 J. Kleinbauer, R. Knappe and R. Wallenstein, *Top. Appl. Phys.*, 2004, **96**, 9–16.
8 D. H. Sutter, G. Steinmeyer, L. Gallmann, N. Matuschek, F. Morier-Genoud, U. Keller, V. Scheuer, G. Angelow and T. Tschudi, *Opt. Lett.*, 1999, **24**, 631–633.
9 U. Morgner, F. X. Kartner, S. H. Cho, Y. Chen, H. A. Haus, J. G. Fujimoto, E. P. Ippen, V. Scheuer, G. Angelow and T. Tschudi, *Opt. Lett.*, 1999, **24**, 411–413.
10 P. M. Paul, E. S. Toma, P. Breger, G. Mullot, F. Auge, P. Balcou, H. G. Muller and P. Agostini, *Science*, 2001, **292**, 1689–1692.
11 R. L. Fork, C. H. B. Cruz, P. C. Becker and C. V. Shank, *Opt. Lett.*, 1987, **12**, 483–485.
12 K. Iga, *IEEE J. Sel. Top. Quantum Electron.*, 2000, **6**, 1201–1215.
13 O. Okhotnikov, A. Grudinin and M. Pessa, *New J. Phys.*, 2004, **6**, art. no. 177.
14 J. Feldhaus, J. Arthur and J. B. Hastings, *J. Phys. B: At., Mol. Opt. Phys.*, 2005, **38**, S799–S819.
15 A. Stingl, C. Spielmann, F. Krausz and R. Szipöcs, *Opt. Lett.*, 1994, **19**, 204–206.
16 R. Szipöcs, K. Ferencz, C. Spielmann and F. Krausz, *Opt. Lett.*, 1994, **19**, 201–203.
17 E. B. Treacy, *IEEE J. Quantum Electron.*, 1969, **5**, 454–458.
18 R. L. Fork, O. E. Martinez and J. P. Gordon, *Opt. Lett.*, 1984, **9**, 150–152.
19 C. LeBlanc, P. Curley and F. Salin, *Opt. Commun.*, 1996, **131**, 391–398.
20 D. Strickland and G. Mourou, *Opt. Commun.*, 1985, **56**, 219–221.
21 E. B. Treacy, *Phys. Lett. A*, 1968, **A28**, 34–35.
22 O. E. Martinez, *IEEE J. Quantum Electron.*, 1987, **23**, 1385–1387.
23 O. E. Martinez, *IEEE J. Quantum Electron.*, 1987, **23**, 59–64.
24 M. Drescher and F. Krausz, *J. Phys. B: At., Mol. Opt. Phys.*, 2005, **38**, S727–S740.
25 M. Nisoli, S. DeSilvestri, O. Svelto, R. Szipöcs, K. Ferencz, C. Spielmann, S. Sartania and F. Krausz, *Opt. Lett.*, 1997, **22**, 522–524.
26 A. Baltuška, T. Udem, M. Uiberacker, M. Hentschel, E. Goulielmakis, C. Gohle, R. Holzwarth, V. S. Yakoviev, A. Scrinzi, T. W. Hänsch and F. Krausz, *Nature*, 2003, **421**, 611–615.
27 J. Seres, E. Seres, A. J. Verhoef, G. Tempea, C. Strelill, P. Wobrauschek, V. Yakovlev, A. Scrinzi, C. Spielmann and E. Krausz, *Nature*, 2005, **433**, 596–596.
28 S. E. Harris and A. V. Sokolov, *Phys. Rev. Lett.*, 1998, **81**, 2894–2897.
29 E. Sali, K. J. Mendham, J. W. G. Tisch, T. Halfmann and J. P. Marangos, *Opt. Lett.*, 2004, **29**, 495–497.
30 A. V. Sokolov, M. Y. Shverdin, D. R. Walker, D. D. Yavuz, A. M. Burzo, G. Y. Yin and S. E. Harris, *J. Mod. Opt.*, 2005, **52**, 285–304.
31 A. M. Weiner, *Prog. Quantum Electron.*, 1995, **19**, 161–237.
32 A. M. Weiner, *Rev. Sci. Instrum.*, 2000, **71**, 1929–1960.
33 D. Goswami, *Phys. Rep.*, 2003, **374**, 385–481.
34 A. M. Weiner, D. E. Leaird, J. S. Patel and J. R. Wullert, *Opt. Lett.*, 1990, **15**, 326–328.
35 A. M. Weiner, D. E. Leaird, J. S. Patel and J. R. Wullert, *IEEE J. Quantum Electron.*, 1992, **28**, 908–920.
36 M. M. Wefers and K. A. Nelson, *Opt. Lett.*, 1993, **18**, 2032–2034.
37 M. M. Wefers and K. A. Nelson, *Science*, 1993, **262**, 1381–1382.
38 G. Stobrawa, M. Hacker, T. Feurer, D. Zeidler, M. Motzkus and F. Reichel, *Appl. Phys. B: Lasers Opt.*, 2001, **72**, 627–630.
39 C. Dorrer, F. Salin, F. Verluise and J. P. Huignard, *Opt. Lett.*, 1998, **23**, 709–711.
40 T. Brixner and G. Gerber, *Opt. Lett.*, 2001, **26**, 557–559.
41 C. W. Hillegas, J. X. Tull, D. Goswami, D. Strickland and W. S. Warren, *Opt. Lett.*, 1994, **19**, 737–739.
42 M. A. Dugan, J. X. Tull and W. S. Warren, *J. Opt. Soc. Am. B*, 1997, **14**, 2348–2358.
43 J. X. Tull, M. A. Dugan and W. S. Warren, *Adv. Magn. Opt. Reson.*, 1997, **20**, 1.
44 M. R. Fetterman, D. Goswami, D. Keusters, W. Yang, J. K. Rhee and W. S. Warren, *Opt. Express*, 1998, **3**, 366–375.
45 P. Tournois, *Opt. Commun.*, 1997, **140**, 245–249.
46 F. Verluise, V. Laude, Z. Cheng, C. Spielmann and P. Tournois, *Opt. Lett.*, 2000, **25**, 575–577.
47 D. Kaplan, P. Tournois, B. Chatel and A. Monmayrant, *Ultrafast Phenomena XIV*, ed. T. Kobayashi, Springer, Berlin, Heidelberg, New York, 2004.
48 A. Monmayrant, A. Arbouet, B. Girard, B. Chatel, A. Barman, B. J. Whitaker and D. Kaplan, *Appl. Phys. B*, 2005, **81**, 177–180.
49 M. Roth, M. Mehendale, A. Bartelt and H. Rabitz, *Appl. Phys. B: Lasers Opt.*, 2005, **80**, 441–444.
50 E. Zeek, K. Maginnis, S. Backus, U. Russek, M. Murnane, G. Mourou, H. Kapteyn and G. Vdovin, *Opt. Lett.*, 1999, **24**, 493–495.
51 G. Chériaux, O. Albert, V. Wänman, J. P. Chambaret, C. Félix and G. Mourou, *Opt. Lett.*, 2001, **26**, 169–171.
52 C. Radzewicz, P. Wasylczyk, W. Wasilewski and J. S. Krasiński, *Opt. Lett.*, 2004, **29**, 177–179.
53 M. Hacker, G. Stobrawa, R. Sauerbrey, T. Buckup, M. Motzkus, M. Wildenhain and A. Gehner, *Appl. Phys. B: Lasers Opt.*, 2003, **76**, 711–714.
54 P. Wnuk, C. Radzewicz and J. S. Krasiński, *Opt. Exp.*, 2005, **13**, 4154–4159.
55 G. Vdovin and M. Loktev, *Opt. Lett.*, 2002, **27**, 677–679.
56 R. A. Bartels, T. C. Weinacht, N. Wagner, M. Baertschy, C. H. Greene, M. M. Murnane and H. C. Kapteyn, *Phys. Rev. Lett.*, 2002, **88**, 1, 013903.
57 G. Agrawal, *Nonlinear Fiber Optics*, Academic Press, San Diego, 3rd edn, 2001.
58 A. Brun, P. Georges, G. Lesaux and F. Salin, *J. Phys. D: Appl. Phys.*, 1991, **24**, 1225–1233.
59 D. J. Kane and R. Trebino, *IEEE J. Quantum Electron.*, 1993, **29**, 571–579.
60 R. Trebino and D. J. Kane, *J. Opt. Soc. Am. A*, 1993, **10**, 1101–1111.
61 R. Trebino, K. W. DeLong, D. N. Fittinghoff, J. N. Sweetser, M. A. Krumbűgel, B. A. Richman and D. J. Kane, *Rev. Sci. Instrum.*, 1997, **68**, 3277–3295.
62 R. Trebino, *Frequency-resolved optical gating: the measurement of ultrashort laser pulses*, Kluwer Academic Publishers, Boston, 2000.
63 C. Iaconis and I. A. Walmsley, *Opt. Lett.*, 1998, **23**, 792–794.
64 C. Iaconis and I. A. Walmsley, *IEEE J. Quantum Electron.*, 1999, **35**, 501–509.
65 P. Londero, M. E. Anderson, C. Radzewicz, C. Iaconis and I. A. Walmsley, *J. Mod. Opt.*, 2003, **50**, 179–184.
66 Z. Wu, H. Loos, Y. Shen, B. Sheehy, E. D. Johnson, S. Krinsky, J. B. Murphy, J. Rose, T. Shaftan, X.-J. Wang and L. H. Yu, *Proceedings of the 26th FEL Conference, Trieste, Italy*, Sincrotrone Trieste (ELETTRA), 2004, pp. 285–288.
67 C. Dorrer, E. M. Kosik and I. A. Walmsley, *Opt. Lett.*, 2002, **27**, 548–550.
68 W. Kornelis, J. Biegert, J. W. G. Tisch, M. Nisoli, G. Sansone, C. Vozzi, S. De Silvestri and U. Keller, *Opt. Lett.*, 2003, **28**, 281–283.
69 D. J. Kane, J. Weston and K. C. J. Chu, *Appl. Opt.*, 2003, **42**, 1140–1144.
70 W. Wohlleben, J. Degert, A. Monmayrant, B. Chatel, M. Motzkus and B. Girard, *Appl. Phys. B: Lasers Opt.*, 2004, **79**, 435–439.

71 K. K. Lehmann and G. Scoles, *Science*, 1998, **279**, 2065–2066.
72 J. P. Toennies and A. F. Vilesov, *Angew. Chem., Int. Ed.*, 2004, **43**, 2622–2648.
73 R. E. Grisenti and J. P. Toennies, *Phys. Rev. Lett.*, 2003, **90**, 234501.
74 N. Portner, A. F. Vilesov and M. Havenith, *Chem. Phys. Lett.*, 2003, **368**, 458–464.
75 S. Curtis, A. Boatwright, R. R. Wright and A. J. Stace, *Chem. Phys. Lett.*, 2005, **401**, 254–258.
76 J. B. Fenn, M. Mann, C. K. Meng, S. F. Wong and C. M. Whitehouse, *Science*, 1989, **246**, 67–71.
77 D. D. Ebeling, M. S. Westphall, M. Scalf and L. M. Smith, *Anal. Chem.*, 2000, **72**, 5158–5161.
78 A. Stolow, A. E. Bragg and D. M. Neumark, *Chem. Rev.*, 2004, **104**, 1719–1757.
79 V. Blanchet, M. Z. Zgierski, T. Seideman and A. Stolow, *Nature*, 1999, **401**, 52–54.
80 S. M. Bellm and K. L. Reid, *Chem. Phys. Lett.*, 2004, **395**, 253.
81 P. Kruit and F. H. Read, *J. Phys. E: Sci. Instrum.*, 1983, **16**, 313.
82 D. H. Paik, I. R. Lee, D. S. Yang, J. S. Baskin and A. H. Zewail, *Science*, 2004, **306**, 672–675.
83 I. Wolf, S. Ronen, R. Giniger and O. Cheshnovsky, *J. Chem. Phys.*, 2005, **122**, 141101.
84 D. W. Chandler and P. L. Houston, *J. Chem. Phys.*, 1987, **87**, 1445.
85 A. T. J. B. Eppink and D. H. Parker, *Rev. Sci. Instrum.*, 1997, **68**, 3477–3484.
86 H. L. Offerhaus, C. Nicole, F. Lepine, C. Bordas, F. Rosca-Pruna and M. J. J. Vrakking, *Rev. Sci. Instrum.*, 2001, **72**, 3245–3248.
87 M. J. J. Vrakking, *Rev. Sci. Instrum.*, 2001, **72**, 4084.
88 O. Gessner, E. T. H. Chrysostom, A. M. D. Lee, D. M. Wardlaw, M. L. Ho, S. J. Lee, B. M. Cheng, M. Z. Zgierski, I. C. Chen, J. P. Shaffer, C. C. Hayden and A. Stolow, *Faraday Discuss.*, 2004, **127**, 193–212.
89 S. Ullrich, T. Schultz, M. Z. Zgierski and A. Stolow, *Phys. Chem. Chem. Phys.*, 2004, **6**, 2796–2801.
90 M. Tsubouchi, B. J. Whitaker and T. Suzuki, *J. Phys. Chem. A*, 2004, **108**, 6823–6835.
91 W. Cheng, N. Kuthirummal, J. L. Gosselin, T. I. Solling, R. Weinkauf and P. M. Weber, *J. Phys. Chem. A*, 2005, **109**, 1920–1925.
92 M. Tsubouchi, C. A. de Lange and T. Suzuki, *J. Electron Spectrosc. Relat. Phenom.*, 2005, **142**, 193–205.
93 M. T. Zanni, V. S. Batista, B. J. Greenblatt, W. H. Miller and D. M. Neumark, *J. Chem. Phys.*, 1999, **110**, 3748–3755.
94 R. Mabbs, K. Pichugin and A. Sanov, *J. Chem. Phys.*, 2005, **122**, 174305.
95 A. E. Bragg, J. R. R. Verlet, A. Kammrath, O. Cheshnovsky and D. M. Neumark, *J. Chem. Phys.*, 2005, **122**, 054314.
96 A. E. Bragg, J. R. R. Verlet, A. Kammrath, O. Cheshnovsky and D. M. Neumark, *Science*, 2004, **306**, 669–671.
97 E. Surber, R. Mabbs, T. Habteyes and A. Sanov, *J. Phys. Chem. A*, 2005, **109**, 4452–4458.
98 R. Mabbs, E. Surber and A. Sanov, *J. Chem. Phys.*, 2005, **122**, 054308.
99 T. M. Bernhardt, J. Hagen, L. D. Socaciu, R. Mitric, A. Heidenreich, J. Le Roux, D. Popolan, M. Vaida, L. Woste, V. Bonacic-Koutecky and J. Jortner, *ChemPhysChem*, 2005, **6**, 243–253.
100 J. A. Davies, R. E. Continetti, D. W. Chandler and C. C. Hayden, *Phys. Rev. Lett.*, 2000, **84**, 5983–5986.
101 J. A. Davies, J. E. LeClaire, R. E. Continetti and C. C. Hayden, *J. Chem. Phys.*, 1999, **111**, 1–4.
102 H. J. Deyerl and R. E. Continetti, *Phys. Chem. Chem. Phys.*, 2005, **7**, 855–860.
103 C.-Y. Ng, *Annu. Rev. Phys. Chem.*, 2002, **53**, 101–140.
104 O. Kittelmann, J. Ringling, G. Korn, A. Nazarkin and I. V. Hertel, *Opt. Lett.*, 1996, **21**, 1159–1161.
105 L. Nugent-Glandorf, M. Scheer, D. A. Samuels, V. Bierbaum and S. R. Leone, *Rev. Sci. Instrum.*, 2002, **73**, 1875–1886.
106 J. D. Ewbank, J. Y. Luo, J. T. English, R. F. Liu, W. L. Faust and L. Schafer, *J. Phys. Chem.*, 1993, **97**, 8745–8751.
107 M. Ben-Nun, T. J. Martinez, P. M. Weber and K. R. Wilson, *Chem. Phys. Lett.*, 1996, **262**, 405.
108 R. Srinivasan, V. A. Lobastov, C. Y. Ruan and A. H. Zewail, *Helv. Chim. Acta*, 2003, **86**, 1763–1838.
109 R. C. Dudek and P. M. Weber, *J. Phys. Chem. A*, 2001, **105**, 4167–4171.
110 J. Cao, Z. Hao, H. Park, C. Tao, D. Kau and L. Blaszczyk, *Appl. Phys. Lett.*, 2003, **83**, 1044–1046.
111 V. A. Lobastov, R. Srinivasan, B. M. Goodson, C. Y. Ruan, J. S. Feenstra and A. H. Zewail, *J. Phys. Chem. A*, 2001, **105**, 11159–11164.
112 R. Srinivasan, J. S. Feenstra, S. T. Park, S. J. Xu and A. H. Zewail, *Science*, 2005, **307**, 558–563.
113 J. M. Cao, H. Ihee and A. H. Zewail, *Proc. Natl. Acad. Sci. U. S. A.*, 1999, **96**, 338–342.
114 H. Ihee, B. M. Goodson, R. Srinivasan, V. A. Lobastov and A. H. Zewail, *J. Phys. Chem. A*, 2002, **106**, 4087–4103.
115 H. Ihee, V. A. Lobastov, U. M. Gomez, B. M. Goodson, R. Srinivasan, C.-Y. Ruan and A. H. Zewail, *Science*, 2001, **291**, 458–462.
116 H. Ihee, J. Cao and A. H. Zewail, *Chem. Phys. Lett.*, 1997, **281**, 10.
117 H. Ihee, J. M. Cao and A. H. Zewail, *Angew. Chem., Int. Ed.*, 2001, **40**, 1532–1536.
118 J. C. Williamson, J. M. Cao, H. Ihee, H. Frey and A. H. Zewail, *Nature*, 1997, **386**, 159–162.
119 J. Cao, H. Ihee and A. H. Zewail, *Chem. Phys. Lett.*, 1998, **290**, 1.
120 H. Ihee, J. S. Feenstra, J. M. Cao and A. H. Zewail, *Chem. Phys. Lett.*, 2002, **353**, 325–334.
121 C. Y. Ruan, V. A. Lobastov, R. Srinivasan, B. M. Goodson, H. Ihee and A. H. Zewail, *Proc. Natl. Acad. Sci. U. S. A.*, 2001, **98**, 7117–7122.
122 T. Zuo, A. D. Bandrauk and P. B. Corkum, *Chem. Phys. Lett.*, 1996, **259**, 313–320.
123 M. Spanner, O. Smirnova, P. B. Corkum and M. Y. Ivanov, *J. Phys. B: At., Mol. Opt. Phys.*, 2004, L243.
124 J. Itatani, J. Levesque, D. Zeidler, H. Niikura, H. Pepin, J. C. Kieffer, P. B. Corkum and D. M. Villeneuve, *Nature*, 2004, **432**, 867–871.
125 S. Jorgensen and R. Kosloff, *Phys. Rev. A*, 2004, **70**, 015602.
126 M. Shapiro and P. Brumer, *J. Chem. Phys.*, 1986, **84**, 4103–4104.
127 M. Shapiro and P. Brumer, *Int. Rev. Phys. Chem.*, 1994, **13**, 187–229.
128 M. Shapiro, J. W. Hepburn and P. Brumer, *Chem. Phys. Lett.*, 1988, **149**, 451–454.
129 N. V. Vitanov, T. Halfmann, B. W. Shore and K. Bergmann, *Annu. Rev. Phys. Chem.*, 2001, **52**, 763–809.
130 M. Shapiro and P. Brumer, *J. Chem. Phys.*, 1986, **84**, 540–541.
131 S. T. Cundiff and J. Ye, *Rev. Mod. Phys.*, 2003, **75**, 325–342.
132 H. Ohmura and T. Nakanaga, *J. Chem. Phys.*, 2004, **120**, 5176–5180.
133 A. J. Wurzer, S. Lochbrunner and E. Riedle, *Appl. Phys. B: Lasers Opt.*, 2000, **71**, 405–409.
134 T. Baumert, M. Grosser, R. Thalweiser and G. Gerber, *Phys. Rev. Lett.*, 1991, **67**, 3753–3756.
135 D. J. Tannor, R. Kosloff and S. A. Rice, *J. Chem. Phys.*, 1986, **85**, 5805–5820.
136 D. J. Tannor and S. A. Rice, *J. Chem. Phys.*, 1985, **83**, 5013–5018.
137 W. S. Warren and A. H. Zewail, *J. Chem. Phys.*, 1981, **75**, 5956–5958.
138 W. R. Lambert, P. M. Felker and A. H. Zewail, *J. Chem. Phys.*, 1981, **75**, 5958–5960.
139 N. F. Scherer, A. J. Ruggiero, M. Du and G. R. Fleming, *J. Chem. Phys.*, 1990, **93**, 856–857.
140 N. F. Scherer, R. J. Carlson, A. Matro, M. Du, A. J. Ruggiero, V. Romero-Rochin, J. A. Cina, G. R. Fleming and S. A. Rice, *J. Chem. Phys.*, 1991, **95**, 1487–1511.
141 M. W. Noel and C. R. Stroud, *Phys. Rev. Lett.*, 1995, **75**, 1252–1255.
142 J. R. R. Verlet, V. G. Stavros, R. S. Minns and H. H. Fielding, *Phys. Rev. Lett.*, 2002, **89**, 263004.
143 R. E. Carley, E. D. Boleat, R. S. Minns, R. Patel and H. H. Fielding, *J. Phys. B: At., Mol. Opt. Phys.*, 2005, **38**, 1907.
144 R. S. Minns, J. R. R. Verlet, L. J. Watkins and H. H. Fielding, *J. Chem. Phys.*, 2003, **119**, 5842–5847.
145 R. S. Minns, R. Patel, J. R. R. Verlet and H. H. Fielding, *Phys. Rev. Lett.*, 2003, **91**, 243601.

146 J. Degert, C. Meier, B. Chatel and B. Girard, *Phys. Rev. A: At., Mol. Opt. Phys.*, 2003, **67**, 041402.
147 M. Wollenhaupt, A. Assion, D. Liese, C. Sarpe-Tudoran, T. Baumert, S. Zamith, M. A. Bouchene, B. Girard, A. Flettner, U. Weichmann and G. Gerber, *Phys. Rev. Lett.*, 2002, **89**, 173001.
148 C. Doule, E. Hertz, L. Berguiga, R. Chaux, B. Lavorel and O. Faucher, *J. Phys. B: At., Mol. Opt. Phys.*, 2001, **34**, 1133–1142.
149 B. Chatel, J. Degert and B. Girard, *Phys. Rev. A: At., Mol. Opt. Phys.*, 2004, **70**, 053414.
150 G. P. Djotyan, J. S. Bakos, Z. Sorlei and J. Szigeti, *Phys. Rev. A: At., Mol. Opt. Phys.*, 2004, **70**, 063406.
151 J. S. Melinger, S. R. Gandhi, A. Hariharan, J. X. Tull and W. S. Warren, *Phys. Rev. Lett.*, 1992, **68**, 2000–2003.
152 J. S. Melinger, S. R. Gandhi, A. Hariharan, D. Goswami and W. S. Warren, *J. Chem. Phys.*, 1994, **101**, 6439–6454.
153 J. S. Melinger, A. Hariharan, S. R. Gandhi and W. S. Warren, *J. Chem. Phys.*, 1991, **95**, 2210–2213.
154 S. Chelkowski, A. D. Bandrauk and P. B. Corkum, *Phys. Rev. Lett.*, 1990, **65**, 2355–2358.
155 D. J. Maas, M. J. J. Vrakking and L. D. Noordam, *Phys. Rev. A*, 1999, **60**, 1351–1362.
156 B. Broers, H. B. V. Vandenheuvell and L. D. Noordam, *Phys. Rev. Lett.*, 1992, **69**, 2062–2065.
157 A. Assion, T. Baumert, J. Helbing, V. Seyfried and G. Gerber, *Chem. Phys. Lett.*, 1996, **259**, 488–494.
158 J. Degert, W. Wohlleben, B. Chatel, M. Motzkus and B. Girard, *Phys. Rev. Lett.*, 2002, **89**, 203003.
159 M. A. Bouchene, C. Nicole and B. Girard, *J. Phys. B: At., Mol. Opt. Phys.*, 1999, **32**, 5167–5177.
160 G. Cerullo, C. J. Bardeen, Q. Wang and C. V. Shank, *Chem. Phys. Lett.*, 1996, **262**, 362–368.
161 C. J. Bardeen, Q. Wang and C. V. Shank, *J. Phys. Chem. A*, 1998, **102**, 2759–2766.
162 K. Misawa and T. Kobayashi, *J. Chem. Phys.*, 2000, **113**, 7546–7553.
163 B. Kohler, V. V. Yakovlev, J. W. Che, J. L. Krause, M. Messina, K. R. Wilson, N. Schwentner, R. M. Whitnell and Y. J. Yan, *Phys. Rev. Lett.*, 1995, **74**, 3360–3363.
164 C. J. Bardeen, J. W. Che, K. R. Wilson, V. V. Yakovlev, V. A. Apkarian, C. C. Martens, R. Zadoyan, B. Kohler and M. Messina, *J. Chem. Phys.*, 1997, **106**, 8486–8503.
165 C. J. Bardeen, J. W. Che, K. R. Wilson, V. V. Yakovlev, P. J. Cong, B. Kohler, J. L. Krause and M. Messina, *J. Phys. Chem. A*, 1997, **101**, 3815–3822.
166 J. C. Davis and W. S. Warren, *J. Chem. Phys.*, 1999, **110**, 4229–4237.
167 S. Sen, S. Ghosh, S. S. Bhattacharyya and S. Saha, *J. Chem. Phys.*, 2002, **116**, 581–588.
168 R. Netz, A. Nazarkin and R. Sauerbrey, *Phys. Rev. Lett.*, 2003, **90**, 063001.
169 B. Y. Chang, I. R. Sola, V. S. Malinovsky and J. Santamaria, *J. Chem. Phys.*, 2000, **113**, 4901–4911.
170 S. Yoshida, C. O. Reinhold, E. Persson, J. Burgd and F. B. Dunning, *J. Phys. B: At., Mol. Opt. Phys.*, 2005, **38**, S209.
171 A. Präkelt, M. Wollenhaupt, C. Sarpe-Tudoran and T. Baumert, *Phys. Rev. A: At., Mol. Opt. Phys.*, 2004, **70**, 063407.
172 T. C. Weinacht, J. Ahn and P. H. Bucksbaum, *Phys. Rev. Lett.*, 1998, **80**, 5508–5511.
173 D. Meshulach and Y. Silberberg, *Phys. Rev. A*, 1999, **60**, 1287–1292.
174 M. Renard, E. Hertz, B. Lavorel and O. Faucher, *Phys. Rev. A*, 2004, **69**, 043401.
175 D. Meshulach and Y. Silberberg, *Nature*, 1998, **396**, 239–242.
176 T. Hornung, R. Meier, D. Zeidler, K.-L. Kompa, D. Proch and M. Motzkus, *Appl. Phys. B: Lasers Opt.*, 2000, **71**, 277–284.
177 I. Pastirk, J. M. Dela Cruz, K. A. Walowicz, V. V. Lozovoy and M. Dantus, *Opt. Express*, 2003, **11**, 1695–1701.
178 C. Rangan, J. Ahn, D. N. Hutchinson and P. H. Bucksbaum, *J. Mod. Opt.*, 2002, **49**, 2339–2347.
179 R. S. Judson and H. Rabitz, *Phys. Rev. Lett.*, 1992, **68**, 1500–1503.
180 T. Baumert, T. Brixner, V. Seyfried, M. Strehle and G. Gerber, *Appl. Phys. B: Lasers Opt.*, 1997, **65**, 779–782.
181 C. J. Bardeen, V. V. Yakovlev, K. R. Wilson, S. D. Carpenter, P. M. Weber and W. S. Warren, *Chem. Phys. Lett.*, 1997, **280**, 151–158.
182 R. Bartels, S. Backus, E. Zeek, L. Misoguti, G. Vdovin, I. P. Christov, M. M. Murnane and H. C. Kapteyn, *Nature*, 2000, **406**, 164–166.
183 T. Ando, T. Urakami, H. Itoh and Y. Tsuchiya, *Appl. Phys. Lett.*, 2002, **80**, 4265–4267.
184 B. J. Pearson, J. L. White, T. C. Weinacht and P. H. Bucksbaum, *Phys. Rev. A*, 2001, **63**, 063412.
185 A. Bartelt, S. Minemoto, C. Lupulescu, S. Vajda and L. Woste, *Eur. Phys. J. D*, 2001, **16**, 127–131.
186 J. B. Ballard, H. U. Stauffer, Z. Amitay and S. R. Leone, *J. Chem. Phys.*, 2002, **116**, 1350–1360.
187 T. Hornung, R. Meier, R. de Vivie-Riedle and M. Motzkus, *Chem. Phys.*, 2001, **267**, 261–276.
188 T. C. Weinacht, J. L. White and P. H. Bucksbaum, *J. Phys. Chem. A*, 1999, **103**, 10166–10168.
189 J. L. White, B. J. Pearson and P. H. Bucksbaum, *J. Phys B: At., Mol. Opt. Phys.*, 2004, **37**, L399.
190 T. C. Weinacht, R. Bartels, S. Backus, P. H. Bucksbaum, B. Pearson, J. M. Geremia, H. Rabitz, H. C. Kapteyn and M. M. Murnane, *Chem. Phys. Lett.*, 2001, **344**, 333–338.
191 D. Zeidler, S. Frey, W. Wohlleben, M. Motzkus, F. Busch, T. Chen, W. Kiefer and A. Materny, *J. Chem. Phys.*, 2002, **116**, 5231–5235.
192 A. Assion, T. Baumert, M. Bergt, T. Brixner, B. Kiefer, V. Seyfried, M. Strehle and G. Gerber, *Science*, 1998, **282**, 919–922.
193 D. Cardoza, F. Langhojer, C. Trallero-Herrero, O. L. A. Monti and T. Weinacht, *Phys. Rev. A: At., Mol. Opt. Phys.*, 2004, **70**, 053406.
194 C. Daniel, J. Full, L. Gonzalez, C. Lupulescu, J. Manz, A. Merli, S. Vajda and L. Woste, *Science*, 2003, **299**, 536–539.
195 R. J. Levis, G. M. Menkir and H. Rabitz, *Science*, 2001, **292**, 709–713.
196 T. Brixner, N. H. Damrauer, P. Niklaus and G. Gerber, *Nature*, 2001, **414**, 57–60.
197 T. Brixner, N. H. Damrauer, B. Kiefer and G. Gerber, *J. Chem. Phys.*, 2003, **118**, 3692–3701.
198 J. L. Herek, W. Wohlleben, R. J. Cogdell, D. Zeidler and M. Motzkus, *Nature*, 2002, **417**, 533–535.
199 J. M. Dela Cruz, I. Pastirk, M. Comstock and M. Dantus, *Opt. Express*, 2004, **12**, 4144–4149.
200 B. J. Pearson, J. L. White, T. C. Weinacht and P. H. Bucksbaum, *Phys. Rev. A*, 2001, **6306**, 063412.
201 R. J. Levis and H. A. Rabitz, *J. Phys. Chem. A*, 2002, **106**, 6427.
202 http://usa.hamamatsu.com/assets/pdf/catsandguides/ppm.pdf.
203 T. Brixner, G. Krampert, T. Pfeifer, R. Selle, G. Gerber, M. Wollenhaupt, O. Graefe, C. Horn, D. Liese and T. Baumert, *Phys. Rev. Lett.*, 2004, **92**, 208301.